Deep–Sea Research II 195 (2022) 105015

Contents lists available at ScienceDirect

Deep-Sea Research Part II

journal homepage: www.elsevier.com/locate/dsr2

Mesozooplankton community distribution on the Agulhas Bank in autumn: Size structure and production

Margaux Noyon [a,*], Alex J. Poulton [b], Sarah Asdar [a], Riaan Weitz [a], Sarah L.C. Giering [c]

[a] Department of Oceanography and Institute for Coastal and Marine Research, Nelson Mandela University, Gqeberha, 6001, South Africa
[b] The Lyell Centre for Earth and Marine Science and Technology, Heriot-Watt University, Riccarton Campus, Edinburgh, EH14 4AP, United Kingdom
[c] National Oceanography Centre, Southampton, SO14 3ZH, United Kingdom

ARTICLE INFO

Keywords:
Cross-shore gradient
Continental shelf
Western boundary current
Size spectrum
ZooScan
AARS activity
Mesozooplankton production

ABSTRACT

The Agulhas Bank on the tip of southern Africa, like other shelf seas, is a relatively productive environment which plays a crucial role in the biology and success of many commercially valuable fish species. Fish and their larvae depend on zooplankton to feed on but, despite their importance, little is known about zooplankton distribution and production on the Agulhas Bank. Here we present results from a survey conducted in March 2019 on the East and Central Agulhas Bank, investigating mesozooplankton abundance, biovolume, taxonomic composition, size distribution (normalised biovolume size spectrum (NBSS) approach) and secondary production. A clear cross-shore gradient was observed with the inner-shelf having higher abundance and biovolume of mesozooplankton dominated by small-size organisms, most likely mirroring higher overall productivity of the coastal waters, while the outer-shelf showed the opposite trend (*i.e.*, low abundance and biovolume; shallow NBSS slopes). This general pattern on the outer-shelf was, however, disturbed in one location (between 24 and 25°E) with a distinguishable mesozooplankton community, most likely linked to the passage of a meander on the inshore side of the Agulhas Current. The Central Agulhas Bank was typified by high mesozooplankton biomass (~4 g C m^{-2}), comparable to upwelling areas and dominated by copepods and doliolids. High copepod biomass was observed in this region before and was linked to a feature called the "Cold Ridge". However, during our survey, no such ridge was observed. The mixed layer depth was relatively deep (>20 m) and high Chlorophyll *a* concentration was measured at depth, despite low net primary production rates. We suggest that this region is prone to other mechanisms such as retention due to cyclonic circulation or processes injecting nutrients in the upper mixed layer that require further research. Secondary production on the Agulhas Bank was in the same range as other shelf seas (0.03–1.55 g C m^{-2} d^{-1}) and was correlated with mesozooplankton biomass. The comparison of primary and secondary production, measured simultaneously, suggested that mesozooplankton exert a significant control on net primary production, and can, in some areas, be food-limited (*e.g.*, Central Agulhas Bank and inshore waters).

1. Introduction

Shelf seas are globally productive environments, providing 10–30% of global primary production despite their small size of only ~7–10% of the global ocean area (Bauer et al., 2013). Shelf seas have a key role in supplying food to sustain many fisheries around the world (Pauly et al., 2002) and, being at the interface between estuaries and the open ocean, they are also nurseries for many fish species. Despite their importance, many continental shelf seas are still understudied, resulting in a poor understanding of their functioning and variability. Being able to understand and predict shelf productivity will allow improved management of marine resources, as well as the implementation of mitigation measures to allow local populations to adapt better to future changes (Bianchi and Skjoldal, 2008).

Along the southern South African coast, the Agulhas Bank (also referred to as 'Bank') is known as one of the nursery grounds for endemic and commercially exploited fish species (Hutchings et al., 2002). While some species spawn on the east coast of South Africa (KwaZulu Natal Bight area) and use the Agulhas Bank as a nursery to grow and mature, other species spawn on the Agulhas Bank and use the west coast of South Africa as a nursery (*i.e.*, the Benguela Upwelling System). A key food source for fish is zooplankton which transfer energy from primary

* Corresponding author.
E-mail address: margauxnoyon@gmail.com (M. Noyon).

https://doi.org/10.1016/j.dsr2.2021.105015
Received 10 June 2021; Received in revised form 10 November 2021; Accepted 9 December 2021
Available online 22 December 2021

producers to higher trophic levels. Understanding the distribution and dynamics of zooplankton in shelf seas is thus important to understand fish populations. Few studies exist on zooplankton populations on the Agulhas Bank, and these are mostly from the 1990s and focus only on copepods (references within Huggett and Richardson, 2000).

The dominant large copepod on the Agulhas Bank is *Calanus agulhensis* (Huggett and Richardson, 2000; Peterson and Hutchings, 1995), which can comprise up to 82% of total copepod biomass (Verheye et al., 1994). Based on few regional studies, biomass of this copepod species seems highest on the central Agulhas Bank (Hutchings et al., 1995). Peterson and Hutchings (1995) suggested that this enhanced biomass of copepods was linked to a periodically occurring hydrographic feature named the "Cold Ridge" (or "Cool Ridge") located off Mossel Bay. This Cold Ridge is identified as a doming of the isotherms along the 100 m isobath and associated with elevated nutrients and chlorophyll *a* (Chl *a*) concentrations (Probyn et al., 1994). However, a relationship between the Cold Ridge and copepods has still not been conclusively examined.

Although the east and central Agulhas Bank (EAB and CAB) are small in area (75,120 km^2), they possess spatial differences due to a complex oceanography with dynamic hydrographic features that influence plankton distribution and the functioning of the shelf ecosystem (reviewed by Probyn et al., 1994). Firstly, the warm oligotrophic Agulhas Current, one of the strongest western boundary currents in the world, flows along the shelf break and contrasts with the coastal environment, which is subject to wind-driven upwelling, in terms of temperature, productivity and current speed (Demarcq et al., 2008; Goschen et al., 2012, 2015; Goschen and Schumann, 1990; Jackson et al., 2012; Lutjeharms et al., 1996; Mazwane et al., this issue, Probyn et al., 1994; Schumann, 1999). The Agulhas Current is also the origin of meanders, Natal pulses and eddies, which propagate on its inshore side and can induce localised upwelling on the mid- and outer-shelf, especially on the EAB (Goschen et al., 2015; Jackson et al., 2012; Lutjeharms et al., 1989, 2000; Malan et al., 2018). Finally, the current and associated mesoscale features can sweep significant amounts of planktonic biomass off the productive continental shelf (Keister et al., 2009; Porri et al., 2014), while recirculation mechanisms drive areas on the inner-shelf of the CAB, inducing retention of water masses (Boyd et al., 1992).

In ecology, size as a functional trait has been extensively used, being easy to measure and strongly influencing metabolic rates and predator-prey interactions (*e.g.*, Andersen et al., 2016; Brown et al., 2004; Gillooly et al., 2001; Kiørboe, 2016; Kiørboe and Hirst, 2014; Visser and Fiksen, 2013). According to the size spectrum theory, based on predator-prey relationships, biomass decreases linearly with size on a log-log scale (Platt and Denman, 1977; Silvert and Platt, 1978). The normalised biomass size spectrum (NBSS) is often used to represent the size structure within an ecosystem, as reviewed by Sprules and Barth (2015). The parameters extracted from the NBSS are inherent properties of the zooplankton community and highlight community patterns which inform on the dynamics of the system (Basedow et al., 2010; Dai et al., 2016; Giering et al., 2018; Marcolin et al., 2013; Noyon et al., 2020; Vandromme et al., 2014; Zhou et al., 2004). For instance, the slope of the linear regression of NBSS indicates the proportion of small organisms compared to large ones, with a steeper slope generally interpreted as a decrease in food availability for higher trophic levels (Brown et al., 2004; Zhou, 2006). As for the fit of the linear regression, it informs on the stability of the environment, with a low linear fit indicating a perturbation to the system, often characterised by the presence of "domes" or "dips" in the NBSS, highlighting potential non-steady state conditions (*e.g.*, García-Comas et al., 2014; Quinones et al., 2003; Rodriguez and Mullin, 1986; Sourisseau and Carlotti, 2006; Zhou, 2006).

Here, we are presenting the taxonomic composition, size structure and productivity of the mesozooplankton community, collected during a cruise in March 2019 on the Agulhas Bank. Though little is known about zooplankton abundance and distribution on the Agulhas Bank, we expected to observe cross-shore and longitudinal gradients. We hypothesised that the inner-shelf would have a different zooplankton community to the outer-shelf, dominated by smaller zooplankton due to higher net primary production (NPP) and associated higher growth rates, while the outer-shelf would have lower zooplankton abundance and biovolume due to the influence of the warm oligotrophic Agulhas Current. We also hypothesised the zooplankton community on the EAB to be different to the rest of the Bank due to the frequent upwelling events and the narrow shelf in this region, and, if present, high copepod abundance on the Cold Ridge area.

2. Material and methods

2.1. Study area and sampling

The Agulhas Bank is a continental shelf of less than 200 m depth on the southern tip of Africa. This shelf is influenced by the Benguela upwelling system on its western side while the eastern and central Agulhas Bank (EAB and CAB) are influenced by the warm Agulhas current, a western boundary current, which flows westward along the shelf break (Lutjeharms, 2006). This study focuses on the EAB and CAB which were defined across the programme as east and west of 24°E, respectively, due to differences in water circulation (Boyd et al., 1992).

A total of 48 stations were sampled along 10 cross-shore transects between 23 and 29 March, 2019 on the RV *Ellen Kuzwayo* (Noyon, 2019) (Supplementary Table 1). The station numbering starts with the transect number (1–12) followed by a second number (1–6, or less) going from inshore to offshore, respectively (Fig. 1). Due to bad weather, transects 1 and 2 had to be shortened and were then interrupted, while transects 3 and 4, planned off Algoa Bay, were entirely cancelled. For this specific cruise, we allocated transect 8, which started on the inner-shelf at 24.03°E, to the EAB. Each Bank was then divided into an eastern (eEAB and eCAB) and western (wEAB and wCAB) part (Fig. 1). To highlight any cross-shore differences, we delimited the inner-shelf as stations shallower than ~100 m, and the outer-shelf stations are those closest to the shelf edge. The stations in between are categorised as mid-shelf.

At each station, a Seabird 911+ CTD (Conductivity, Temperature, Depth) rosette, equipped with fluorescence and turbidity sensors, was deployed. The fluorescence sensor was calibrated against discrete samples of Chl *a* measured on a Turner-Designs Trilogy Laboratory Fluorometer, with a non-acidification module following Welschmeyer (1994). In this study, the mixed layer depth (MLD) was determined as the depth of the maximum buoyancy frequency (Carvalho et al., 2017). There is a good agreement between the MLD calculated as the maximum buoyancy frequency and as the depth where the difference between the surface and deeper waters is 0.125 kg m^{-3} (Poulton et al., this issue). The bottom mixed layer (BML) depth was calculated using the threshold of 0.02 kg m^{-3} from the bottom density value (Hopkins et al., 2021). Mesozooplankton samples were collected using a vertical Bongo net (0.25 m^2 mouth area) of 200 μm mesh size equipped with a flowmeter (Hydrobios) and a depth sensor. The depth sensor failed at some stations, in which case the depth was estimated based on the wire out and the volume filtered. The nets were towed in the first 200 m of the water column or down to ~5–15 m above the seafloor where the bottom depth was shallower than 200 m and were performed during day and night. One net sample was preserved in buffered formaldehyde (4% final concentration, buffered with borax) while the other net sample was poured into three Eppendorf tubes (2 mL), flash frozen in liquid nitrogen and preserved at −80°C until further analyses.

2.2. Mesozooplankton community measurements

The formaldehyde preserved samples were used to quantitatively measure abundance and biovolume of mesozooplankton using a Hydroptic ZooScan (resolution of 2400 dpi) (Gorsky et al., 2010). All samples were size-fractionated using a 2 mm sieve, and both fractions were scanned separately. The number of individual mesozooplankton in

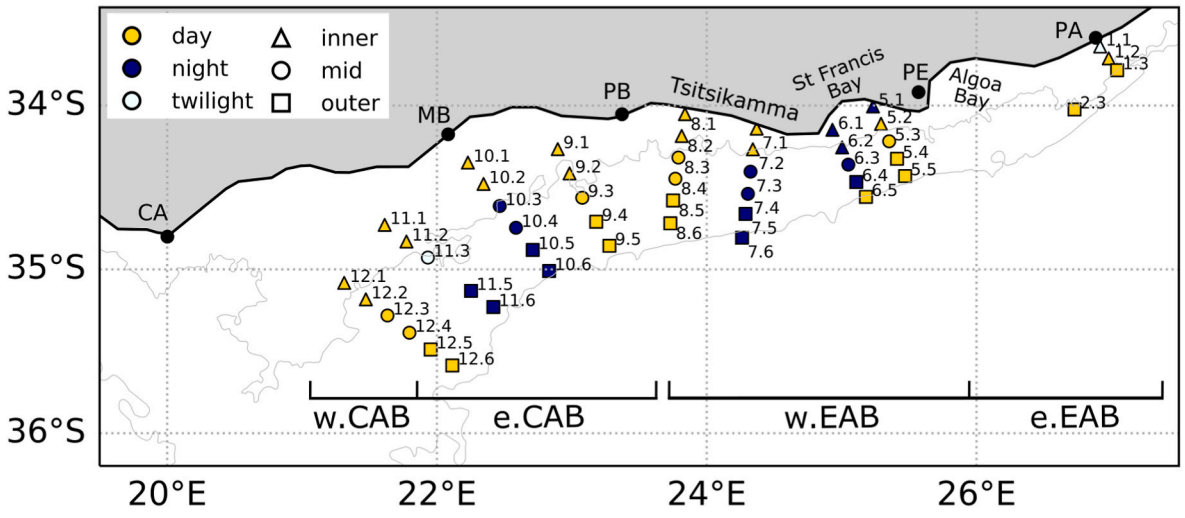

Fig. 1. Map of the stations sampled during the March 2019 cruise on the Agulhas Bank. The stations are divided into inner-, mid- and outer-shelf (symbols) as well as according to their longitude: East and Central Agulhas Bank (EAB and CAB, respectively) which are split into west (w.) and east (e.) sections. The colours yellow for daytime, dark blue for night-time and light blue for twilight correspond to the time of the day when the Bongo net samples were collected. The grey lines represent the 100 and 200 m isobath, the latter corresponding to the shelf break. (PA: Port Alfred, PE: Port Elizabeth (now Gqeberha), PB: Plettenberg Bay, MB: Mossel Bay, CA: Cape Agulhas). (For interpretation of the references to colour in this figure legend, the reader is referred to the Web version of this article.)

the smaller fraction often exceeded the recommended number for ZooScan processing (1000–1500 ind.) and was split (using a MOTODA splitter) until the recommended particle number was reached. The whole of the large fraction was scanned. The raw images were processed using ZooProcess and digitally separated when needed as recommended (Vandromme et al., 2012). The segmented images ('vignettes') were automatically classified into taxa using EcoTaxa's deep-learning algorithm (Picheral et al., 2017). The automated classification results were manually checked and corrected when needed. The volume of each particle (mm^3) was calculated assuming an ellipsoid using the major and minor axes of each particle. The abundance (ind m^{-3}) and biovolume (mm^3 m^{-3}) were then calculated based on the split and the volume of seawater filtered. Due to the differences in depth along the shelf, integrated abundance and biovolume are mostly used in this work; these were obtained by multiplying the abundance and biovolume by the measured depth of the plankton net tow. Data are available (Noyon, 2021; https://www.bodc.ac.uk/data/published_data_library/catalogue/10.5285/cd9da2f5-05f6-15bb-e053-6c86abc01d68/).

We included all zooplankton images to estimate total abundance and biovolume. Images were grouped into a final number of 16 categories. The category "Harosa" comprised many protists, such as Radiolaria, Foraminifera, and Phaeodaria. Harosa was removed from the nMDS as it had too much weight on the ordination, while most of these organisms were smaller than the 200 μm net mesh and likely to be underestimated. The group "Other copepods" comprised Harpacticoida, Corycaeidae, Sapphirinidae, Lubbockiidae, and copepods whose genus were not identifiable. The group "Other crustaceans" consisted of the taxa Cladocera, Cumacea, Amphipoda, and Ostracoda. Calanoid copepods were divided into 3 subgroups according to their size and approximate development stage. Size thresholds for these development stages were chosen based on the measurements by Huggett et al. (2009): small Calanoida (primarily copepodites C1 and C2) with an equivalent spherical diameter (ESD) of <0.45 mm; medium Calanoida (primarily copepodites C3 and C4) with an ESD between 0.45 and 0.80 mm; and large Calanoida (primarily C5 and adults) with an ESD >0.80 mm.

Size spectra were calculated for each station based on 14 size bins logarithmically increasing from a volume of 0.0098 mm^3 (~0.27 mm ESD) to 857 mm^3 (~11.8 mm ESD), the minimum and maximum bin edges being 0.0058 mm^3 (~0.22 mm ESD) and 1211 mm^3 (~13.2 mm ESD), respectively. The normalised biovolume size spectrum (NBSS) was computed by plotting the $\log_{10}$ of the total biovolume in each bin divided by the volume of that bin (in m^{-3} on the y-axis) against the $\log_{10}$ of the biovolume of the size bins (in mm^3 on the x-axis) (Platt and Denman, 1977; Zhou and Huntley, 1997). A linear regression using the least square method was fitted to the NBSS data for the size bins comprised between 0.48 and 3.67 mm ESD (biovolume equivalent ~ $\log_{10}(-1.25)$ to $\log_{10}(1.41)$). Outside these limits, the biomass spectrum indicated drops in biovolume, likely due to bias in the sampling method, indicating that these extreme size bins were not properly represented. They were therefore not considered in the calculation of the linear regression. The smallest size bin was chosen as the mode of the NBSS (García-Comas et al., 2014) while the largest one was where a drop off was noticed (too few occurrences of organisms). A steep NBSS slope (more negative) indicates a higher proportion of small plankton compared to large ones, while the intercept mirrors the total biomass (Basedow et al., 2010; Dai et al., 2016; García-Comas et al., 2014; Giering et al., 2018; Noyon et al., 2020; Zhou, 2006). The linear fit was used as an indicator of the stability of the system with a low linear fit often indicating the presence of irregularity in the NBSS (*e.g.*, domes and dips; Zhou, 2006).

A size diversity index was calculated based on the Shannon diversity index using the probability density function of the size (Quintana et al., 2008, 2016). The R script "SizeDiversity_2018" programmed by J. J. Egozcue and O. Martínez-Abella was used to compute this index (2020, https://limnolam.org/the-measurement-of-size-diversity/). Size diversity indices are often more sensitive to size changes within a community than simple linear regression as they will take into consideration the domes and dips that can exist in NBSS.

2.3. Mesozooplankton production measurements

Mesozooplankton production rates were estimated using enzyme activities. The activity of the aminoacyl-tRNA synthetases (AARS) is involved in the first step of protein synthesis and is correlated with zooplankton growth (Yebra et al., 2017a). Frozen samples (three replicates per station) were homogenised using an ultrasonic probe (2 min with sample in ice and pulsed sound to avoid warming of the sample) in 4–5 mL of ice-cold Tris buffer pH 7.8. The homogenate was then centrifuged for 10 min at 5000 rpm and 0°C. The AARS activity was measured following the methods by Yebra and Hernández-León (2004) and Yebra et al. (2011), and adapted to a 96-well plate reader (Yebra et al., 2017a). Enzyme activity was measured at 340 nm every 10 s for

20 min at 25°C. The first 3 to 5 min of the reaction were discarded due to reaction equilibrium. The water and the pyrophosphate reagent were dispensed into the 96-well plate prior to the sample and kept at 25°C for 10 min to acclimate and ensure the assay was done at 25°C. The protein concentration in each sample was determined on the same aliquot with the modified Lowry method (Lowry et al., 1951; ThermoScientific Kit), using Bovin Serum Albumin as standard. Specific AARS (spAARS) was calculated as per McKinnon et al. (2015) and corrected for the *in situ* temperature (mean over the whole water column) using the Arrhenius equation with an activation energy of 8.57 kcal mol^{-1} (Yebra et al., 2005).

To estimate zooplankton production, carbon biomass was estimated based on the ZooScan measurements. The dry weight (DW) and carbon biomass were calculated per taxonomic group categories, using allometric relationships found in Garijo and Hernández-León (2015; based on Kiørboe, 2013; Lehette and Hernández-León, 2009, Table 1). Mesozooplankton production rates (ZP in g C m^{-2} d^{-1}) were estimated based on spAARS and the carbon biomass, following the methods by Garijo and Hernández-León (2015). In summary, specific growth (G_{AARS} in day^{-1}) was converted from spAARS using: $G_{AARS} = -0.0117 + 0.0038$ spAARS. Mesozooplankton community production was then calculated using two equations: $ZP_{Hirst} = (0.636 \times G_{AARS} + 0.009) \times$ carbon biomass (based on Hirst et al., 2003); and $ZP_{Garijo} = (0.946 \times G_{AARS} + 0.013) \times$ carbon biomass (based on Garijo and Hernández-León, 2015). The first equation was obtained using a wide-spread dataset from various latitudes and slightly underestimates ZP from subtropical regions when compared to estimations using the second equation which was only based on subtropical samples (Garijo and Hernández-León, 2015). Because the Agulhas Bank is not a tropical environment but has upper ocean water temperatures >18°C, we chose to present the average of these two ZP estimations. The other equations in Garijo and Hernández-León (2015) are not presented here as they tend to underestimate ZP in oligotrophic environments or were similar to those used here.

2.4. Data analyses

Differences in terms of abundance and biovolume between regions (eEAB – wEAB – eCAB - wCAB; and inner – mid - outer-shelf) were tested using the non-parametric Kruskal-Wallis test (KW) and correlations were done using the Spearman coefficient (r_s) as the data were not normally distributed. The Bongo nets were towed in the whole water column, catching similarly mesozooplankton diel vertical migrators at depth during the day and those closer to the surface during night-time. The integrated abundances and biovolumes of the night samples were not significantly higher than the daytime samples (KW, $p > 0.05$) and therefore diel vertical migration was not further considered as a factor in the data analyses. The mesozooplankton taxonomic composition was investigated using non-metric multidimensional scaling (nMDS; metaMDS function of the vegan R package). Briefly, the biovolume data were square root transformed, standardised with a Wisconsin double standardization, and the Bray-Curtis dissimilarity matrix calculated.

Table 1
Relationships between body area (A) and dry weight (DW); and carbon to DW conversion factor used to estimate carbon biomass of the mesozooplankton. Based on Lehette and Hernández-León (2009); Garijo and Hernández-León (2015) and Kiørboe (2013).

Taxa	DW	Carbon:DW conversion factor
Copepods	$43.97 \times A^{1.52}$	0.48
Chaetognaths	$23.45 \times A^{1.19}$	0.361
Euphausiid-like	$49.58 \times A^{1.48}$	0.419
Thaliacea & Medusae[a]	$4.03 \times A^{1.24}$	0.051
Siphonophores	$43.17 \times A^{1.02}$	0.051
Other zooplankton	$43.38 \times A^{1.54}$	0.435

[a] Relationship in Lehette and Hernández-León (2009) only.

More details on the R package can be found in metaMDS help package (Oksanen et al., 2020). The stress of the solution was 0.19, which implies weak links between samples but still reliable conclusions. To test if the taxa composition differed in the different regions, we used a Permanova test (*adonis* function in R) on the same Bray-Curtis matrix as the one used for the nMDS. Significant differences between groups identified by the Permanova test indicate differences in the population average (*i.e.,* the centroid) and the population variance (*i.e.,* the dispersion of the points). To test whether dispersion differed between groups, we applied the *betadisper* function and a *permutest* (R – vegan package). We used the *envfit* function (Vegan R package) to overlay environmental parameters onto the ordination as vectors. These vectors represent the maximum correlation between the projections of the stations onto these vectors and the corresponding variable. Only vectors with significant correlation are shown ($p < 0.05$). We tested nine parameters: temperature at 30 m, sea surface temperature (SST), MLD, BLD, integrated Chl *a* over the whole water column or 200 m when deeper, net primary production (NPP, from Poulton et al., this issue), mesozooplankton total integrated biovolume (BV) and ZP. Other environmental parameters were considered but not included due to their autocorrelation with one of the nine selected variables. Analyses of covariance (ANCOVA) were used to compare the NBSS slopes of the different zones tested. All the plots and data analyses were performed using Python, except when the specific R packages as described above were used. Significance was defined as $p < 0.05$.

3. Results

3.1. Environmental conditions on the Agulhas Bank

In situ measured SST on the shelf varied from 17.3 to 22.4°C with the cooler SST found on transect 7 (Fig. 2). The coldest temperature throughout the water column was observed on transects 5 and 6 (7.5°C), off St Francis Bay. Overall, we noticed a deepening of the MLD from east (~10 m depth) to west on the Agulhas Bank (~25 m depth).

The Chl *a* concentration within the MLD was on average 2.1 mg m^{-3} with a maximum of 10.2 mg m^{-3} on transect 12 (Fig. 2). Off Port Alfred, the MLD was deeper inshore than offshore with a relatively high concentration of integrated Chl *a* (118 mg m^{-2} over the whole water column). Transect 7, which depicted a clear shoaling of the MLD, had relatively high Chl *a* concentration across the whole transect (3.1 mg m^{-3} avg in MLD; Fig. 2). Transects 9 and 10 had low Chl *a* concentration (avg. 1.32 mg m^{-3} in MLD; Fig. 2), while the maximum values were measured on transects 12 with 5.21 mg m^{-3} on average in the MLD at station 12.1 and 196 mg m^{-2} integrated over the whole water column. Transects 11 and 12 were distinct from the others by a deep MLD, a deep Chl *a* maximum between 30 and 40 m and high integrated Chl *a* (85.1 and 115.9 mg m^{-2} on average respectively).

3.2. Mesozooplankton distribution and taxa composition

On average (±standard error; s.e.), over the whole Bank, mesozooplankton integrated abundance was 154.1 (±3.6) $\times 10^3$ ind m^{-2} and integrated biovolume was 56.8 (±1.1) $\times 10^3$ mm^3 m^{-2} (Table 2). Higher mesozooplankton abundance and biovolume were found at the inner-shelf stations compared to the outer-shelf (Fig. 3; see also Supplementary Fig. 1). The abundance on the inner-shelf (35.6–712.5 $\times 10^3$ ind m^{-2}) was statistically higher than on the outer-shelf (5.6–163.7 $\times 10^3$ ind m^{-2}; $KW_{cross\text{-}shore}$ $p < 0.001$) but the mid-shelf was not significantly different from the rest. On the CAB, the biovolumes were higher on the inner-shelf (33.3–172.4 $\times 10^3$ mm^3 m^{-2}) compared to the outer-shelf (15.8–67.6 $\times 10^3$ mm^3 m^{-2}; $KW_{cross\text{-}shore}$ $p < 0.05$) but no such difference was observed on the EAB with an average (±s.e.) value of 45.6 (±2) $\times 10^3$ mm^3 m^{-2} ($KW_{cross\text{-}shore}$ $p = 0.40$).

In terms of carbon, average (±s.e.) estimated mesozooplankton biomass over the EAB and CAB was 1.04 ± 0.02 g C m^{-2}, ranging from

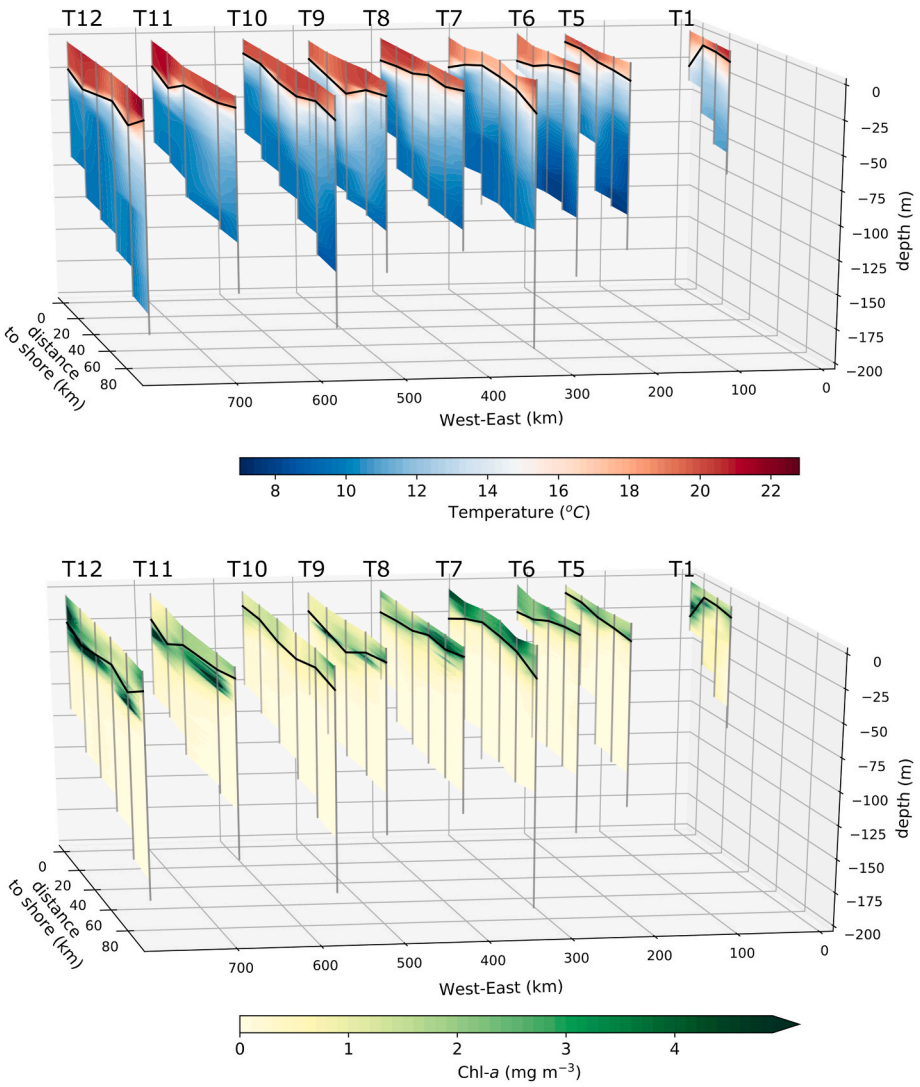

Fig. 2. 3-D representation of temperature (°C, top panel) and chlorophyll *a* (Chl *a* in mg m^{-3}, bottom panel) over the Agulhas Bank in March 2019 from Port Alfred (East, right hand side) to the West (left hand side). The grey vertical lines correspond to the CTD casts and the black lines show the mixed layer depth based on the maximum buoyancy frequency (N^2). T1 to T12 correspond to the transect numbers.

Table 2
Sumary table (average (avg.) ± standard error (se), minimum and maximum values) of zooplankton community parameters for all stations.

All stations (*n = 48)*	Avg. ± se	Min.	Max.
Abundance (ind m^{-3})	2045 ± 51	57	10402
Int. abundance (10^3 ind m^{-2})	154.1 ± 3.6	5.6	712.5
Int. biovolume (10^3 mm^3 m^{-2})	56.8 ± 1.1	4.4	249.4
Int. dry biomass (g m^{-2})	2.41 ± 0.05	0.26	10.36
Int. Carbon biomass (g C m^{-2})	1.04 ± 0.02	0.10	4.27
NBSS – Slope	−0.99	−1.42	−0.35
NBSS – Intercept	1.54	0.77	2.58
NBSS - R^2	0.65	0.43	0.98
Size diversity	2.6 ± 0.01	2.0	3.0
spAARS (nmol PPi hr^{-1} mg $prot^{-1}$)	90.8 ± 0.6	41.3	203.4
Int. ZP (g C m^{-2} d^{-1})	0.27 ± 0.01	0.03	1.55
ZP (mg C m^{-3} d^{-1})	0.176 ± 0.004	0.020	1.162

Int.: integrated, NBSS: Normalised Biovolume Size Spectrum; spAARS: specific aminoacyl-tRNA synthetases; ZP: Zooplankton Production.

0.1 to 4.27 g C m^{-2} (avg. ± s.e.: 12.08 ± 0.26 mg C m^{-3}; min – max: 2.01–54.60 mg C m^{-3}; Table 2). The mesozooplankton biomass revealed a similar trend to the biovolume (r_s = 0.94, $p < 0.001$), with a few exceptions such as stations 12.3 and 12.4 which only had average biomass due to the high biovolume of doliolids (tunicates with high water content; Lehette and Hernández-León, 2009).

Longitudinally, average (±s.e.) abundance and biovolume of mesozooplankton were more elevated on the wCAB compared to any other region (395.8 ± 33.6 × 10^3 ind m^{-2} and 131.2 ± 7.5 × 10^3 mm^3 m^{-2}, respectively: KW_{long} $p < 0.02$). The abundances within the EAB (~94 × 10^3 ind m^{-2}) were similar but the eEAB had significantly lower biovolume compared to the other areas (13.2 ± 1.9 × 10^3 mm^3 m^{-2}; KW_{long} $p < 0.01$). The eCAB and wEAB were significantly different from each other in terms of abundance (142.3 ± 7.0 and 96.6 ± 6.3 × 10^3 ind m^{-2}, respectively; KW_{long} $p < 0.05$) but not in terms of biovolume (41.7 ± 1.5 and 51.5 ± 2.5 × 10^3 mm^3 m^{-2}, respectively; KW_{long} $p = 0.99$).

Overall, large Calanoida represented 36% of the total biovolume, followed by Chaetognatha (13%), Euphausiacea (11.5%) and Thaliacea (10.7%, Fig. 4). For Calanoida, all three size classes included represented on average 44% of the total biovolume. At some stations, the proportion of Calanoida was much lower, often due to the presence of Euphausiacea (*e.g.*, station 7.3), Thalaciacea (*e.g.*, station 12.3), and medusae (*e.g.*, station 7.5), while some stations had a more diverse composition (*e.g.*, station 6.1). The nMDS, computed on the integrated biovolumes of each taxa, revealed a clear inshore-offshore trend and

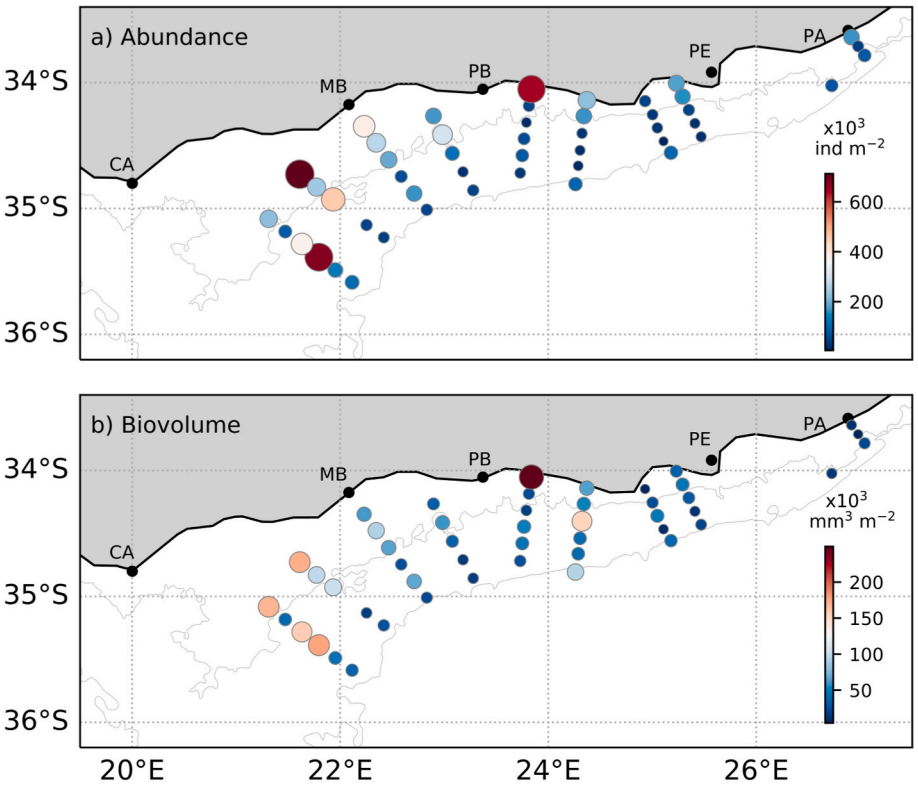

Fig. 3. Mesozooplankton (a) integrated abundance ($\times 10^3$ ind m^{-2}) and (b) integrated biovolume (mm^{-3} m^{-2}) on the Agulhas Bank in March 2019. The size of the dots is proportional to the value of each variable represented.

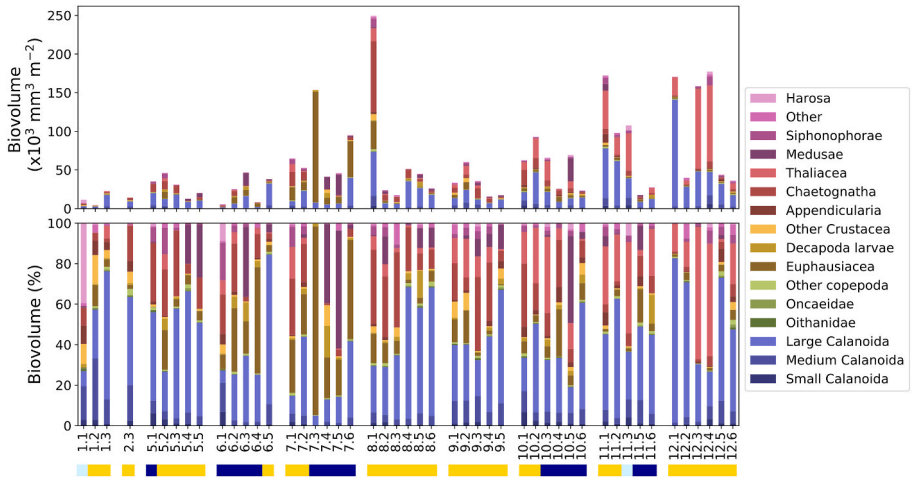

Fig. 4. Bar plot of the biovolume (top panel in $\times 10^3$ mm^3 m^{-3} and bottom panel in %) of all the taxa at all the stations sampled in March 2019 on the Agulhas Bank. The colours at the bottom correspond to the time of sampling with daytime in yellow, night-time in dark blue and twilight in light blue. (For interpretation of the references to colour in this figure legend, the reader is referred to the Web version of this article.)

differences amongst the different regions of the Bank (Fig. 5). Communities were significantly different between the outer- and inner-shelf (Fig. 5c and Supplementary Fig. 2; Permanova $p = 0.001$), while the composition at the stations of the mid-shelf was more variable (*Permutest* $p < 0.05$). The outer-shelf communities had a higher biovolume contribution of copepods (large Calanoida, Oncaea and other copepods) and medusae while the inner-shelf was more diverse with similar proportions of Thalaciacea and Chaetognatha (Fig. 5a and b; Supplementary Fig. 2).

Longitudinally, mesozooplankton communities on the wCAB were clearly distinguishable from the rest of the Bank (Fig. 5d), with a higher biovolume of Thalaciacea (<2 mm ESD) and large Calanoida (Fig. 5b). The communities on the wEAB and the eCAB were statistically indistinguishable (Fig. 5d; *Permutest* and Permanova $p < 0.05$). The mesozooplankton communities on the eEAB were very variable compared to those in the other areas (Fig. 5d) considering that these transects covered a relatively short distance and small area, with clearly different communities at the inshore stations (1.1 and 1.2) compared to the offshore stations (1.3 and 2.3). The mesozooplankton composition at stations 1.1 and 1.2 were similar to station 6.1 and were noticeably different from those at the other stations by the almost total absence of large taxa (Figs. 4 and 5). We observed several stations with 'unique'

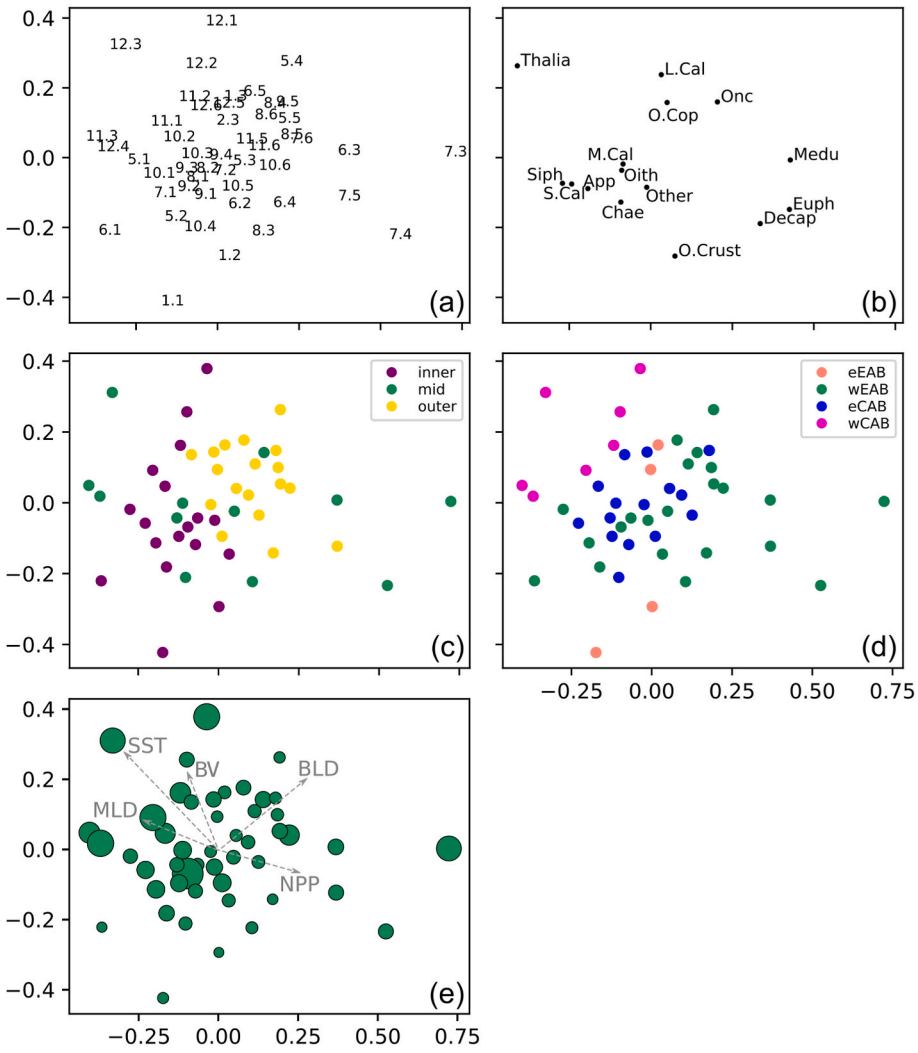

Fig. 5. Ordination of the mesozooplankton samples based on a non-metric multidimensional scaling (nMDS) on integrated biovolume over the whole water column (or down to 200 m when deeper) of all the taxa (stress = 0.19). Pannels a and b represent the stations and the taxa, respectively, in 2D space (App: Appendicularia; S., M., L.Cal: Small, Medium, Large Calanoida; Chae: Chaetognatha; Decap: Decapoda larvae; Euph: Euphausiacea; Medu: Medusae; Oith: Oithonidae; Onc: Oncaeidae; O.Cop: Other Copepoda; O.Crust: Other crustacea; Siph: Siphonophorae; Thalia: Thaliacea). Pannels c, d and e show only the stations (dots) overlaid with the inner/mid/outer-shelf (c), the longitudinal zones (d; eEAB and wEAB: eastern and western East Agulhas Bank; eCAB and wCAB: eastern and western Central Agulhas Bank), and the integrated biovolume represented by the size of the dots (e). The significant environmental variables fitted using the *envfit* function are shown on pannel e ($p < 0.05$ grey dotted arrows, MLD: Mixed Layer Depth based on the maximum boyancy, SST: Sea surface temperature, BV: zooplankton total integrated biovolume, BLD: Bottom mixed layer depth, NPP: Net Primary Production from Poulton et al., this issue).

mesozooplankton community compositions indicated by the large inter-sample distances on the nMDS. Station 7.3 (on the far-right hand-side of the ordination) was characterized by a high biovolume of Euphausiacea, leading to the low abundance and high biovolume described earlier (Figs. 3 and 5d). Stations 6.3, 7.4 and 7.5 were closer to station 7.3 on the ordination and had a high biovolume of Euphausiacea and medusae (Figs. 4, 5a and 5b). The mesozooplankton community at station 8.1, despite having the highest abundance and biovolume, appeared to be relatively typical of the entire shelf region (Fig. 5a). Overall, there was a slight trend of total biovolume being higher for the stations on the upper-left corner of the ordination as confirmed with the *envfit* function ($p = 0.04$, Fig. 5e) although some exceptions occurred, such as station 7.3 which had a high biovolume but a different mesozooplankton composition to the other stations.

Four environmental parameters were significantly related to community composition: MLD, SST, BLD and NPP (Fig. 5e). The BLD is, most likely, highlighting the grouping of the outer-shelf stations which had deeper BLD compared to the inshore stations, while the MLD and SST, which were slightly correlated to each other ($r_s = 0.32$), showed a westward trend of increasing SST associated with a deepening of the MLD. Hence stations with high SST and deep MLD (in the west) appeared to be linked to a higher contribution of Thaliacea and large Calanoida, leading to higher total biovolumes (as shown by the "BV" vector in Fig. 5e). The NPP indicated an opposite trend to SST and MLD with lower NPP values on the wCAB compared to the other regions. The higher NPP were thus not linked to the higher total biovolumes and were more closely associated with the stations dominated by medusae, Euphausiacea and decapoda larvae.

3.3. Size distribution

The overall NBSS of the mesozooplankton size spectra had a slope of −0.99 ($p < 0.001$, $R^2 = 0.65$, $n = 48$; Table 2) and showed recognisable spatial patterns (Fig. 6). The overall NBSS slopes on the inner- (−1.15) and mid-shelf (−0.85) were significantly different from those on the outer-shelf (−0.95, Ancova, $p < 0.001$, Fig. 7) while the inner- and mid-shelf were not statistically different from each other, most likely due to high variability of the mid-shelf stations (Ancova, $p = 0.051$). The mesozooplankton size spectra on the eEAB had a steep slope (−1.39). As per the other parameters, the wEAB and the eCAB revealed similar slopes with intermediate values of −0.79 and −1.02, respectively (Ancova, $p = 0.64$) while the wCAB was characterised by the steepest NBSS slopes of −1.43. The NBSS slopes on the eEAB and wCAB were statistically different from each other (Ancova, $p < 0.001$), although the number of samples on the eEAB is relatively small ($n = 4$) and caution should be taken when interpreting this difference of covariance. Station 7.3 had a very low linear fit of $R^2 = 0.43$ (Fig. 6a), partly because of a dome in the NBSS formed by the Euphausiacea in the large size bins 2.7–3.7 mm ESD (not shown). The linear fit was otherwise relatively high at most stations with $R^2 > 0.8$. The NBSS slopes were negatively correlated with abundance ($r_s = -0.63$, $n = 48$, $p < 0.001$) but not with biovolume, while the NBSS intercept was correlated with both

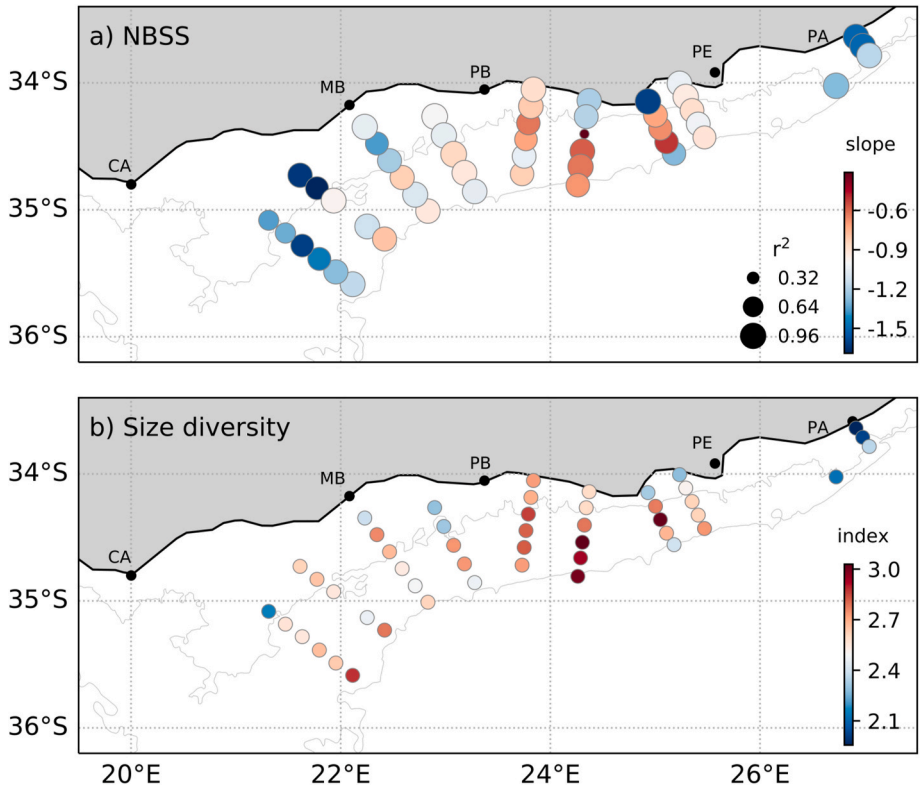

Fig. 6. (a) Slopes of normalised biovolume size spectrum (NBSS, colorbar) overlaid with the linear fit of the NBSS (NBSS R^2, dot size). (b) Size diversity calculated based on the kernel size distribution of all the organisms.

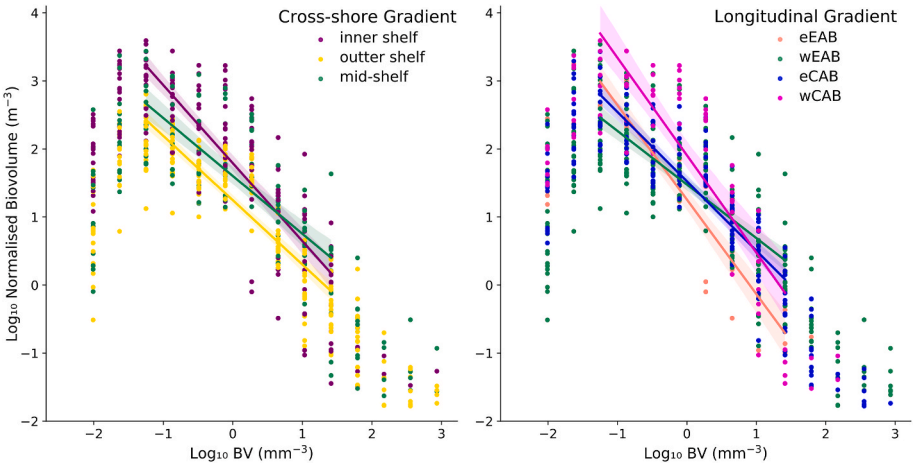

Fig. 7. Normalised biovolume size spectrum for all the stations color coded according to the *a priori* zones: inner, mid and outer-shelf (left panel) and longitudinal zones (right panel; eEAB: eastern East Agulhas Bank, wEAB: western East Agulhas Bank, eCAB: eastern Central Agulhas Bank, wCAB: western Central Agulhas Bank). Average slopes are given for the different inner-to-outer-shelf and regional zones on the Agulhas Bank. (For interpretation of the references to colour in this figure legend, the reader is referred to the Web version of this article.)

abundance and biovolume ($r_s = 0.89$ and 0.71, respectively, $p < 0.001$, $n = 48$).

Size diversity was limited to values between 2 and 3, with the lowest values on the eEAB (2.12 ± 0.04) and at the inner-shelf stations (2.46 ± 0.01; Fig. 6b; $KW_{cross\text{-}shore}$ $p < 0.05$). The highest size diversity indices were found along transect 7, especially at the offshore stations and station 6.3 which were characterized by high biovolumes of Euphausiacea and medusae as described previously (Figs. 4 and 5). Size diversity was correlated to zooplankton abundances ($r_s = -0.4$, $p < 0.01$) and NBSS slopes ($r_s = 0.61$, $p < 0.001$).

3.4. Mesozooplankton enzyme activity and production

Mesozooplankton spAARS activity was on average (±s.e.) 90.8 (±0.6) nmol PPi hr^{-1} mg $prot^{-1}$, varying from 41.3 to 203.4 nmol PPi hr^{-1} mg $prot^{-1}$ (Fig. 8a). The average (±s.e.) spAARS on the EAB was significantly higher than on the CAB (102.6 ± 1.1 and 76.9 ± 0.8 nmol PPi hr^{-1} mg $prot^{-1}$, respectively), mostly due to the high values found on transect 6, and especially at station 6.4 (203.4 nmol PPi hr^{-1} mg $prot^{-1}$). The lowest spAARS were observed on the wCAB (65.6 ± 3.3 nmol PPi hr^{-1} mg $prot^{-1}$; Fig. 8a). The spAARS activity was not significantly correlated with the NBSS slope ($p = 0.06$; $n = 47$; station 7.3 was removed as NBSS linear fit was <0.5), mesozooplankton abundance or biovolume ($p > 0.7$).

The average (±s.e.) estimated mesozooplankton production (ZP) averaged 0.27 (±0.01) g C m^{-2} d^{-1} and 0.18 (±0.004) mg C m^{-3} d^{-1} on the Agulhas Bank in March. The integrated ZP varied greatly from 0.03 to 1.55 g C m^{-2} d^{-1} (Fig. 8b). Integrated ZP was significantly correlated with

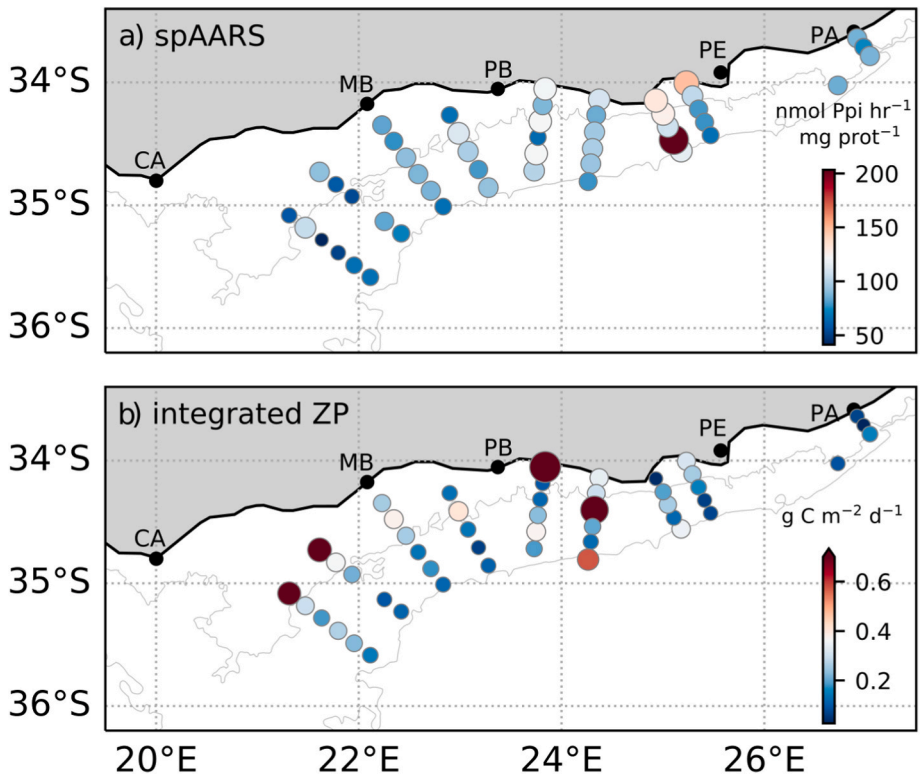

Fig. 8. (a) Mesozooplankton spAARS activity (nmol PPi hr^{-1} mg prot^{-1}) equivalent of zooplankton growth. (b) Integrated mesozooplankton production (g C m^{-2} d^{-1}; note that the colobar has been reduced to show the variability amongst the lower values of production, the maximum value is 1.5 g C m^{-2} d^{-1}). Dot size is proportional to the variable.

carbon biomass ($r_s = 0.92$, $p < 0.001$) and the NBSS intercept ($r_s = 0.63$, $p < 0.001$). Hence high ZP were usually found at stations with high biomass (*e.g.*, stations 7.3, 8.1, 11.1, and 12.1). The eEAB had the lowest integrated ZP (0.08 ± 0.01 g C m^{-2} d^{-1}) while the wCAB had the highest values (0.40 ± 0.04 g C m^{-2} d^{-1}; Fig. 8b).

4. Discussion

4.1. Comparison with other continental shelves

The total mesozooplankton biomass on the Agulhas Bank during this cruise (average ± s.e.: 1.04 ± 0.02 g C m^{-2}) was similar to other continental shelf seas, for example, 0.72–1.24 g C m^{-2} in the Yellow Sea (Sun et al., 2010) and 0.25–1.8 g C m^{-2} in the Celtic Sea (Giering et al., 2018). Mesozooplankton abundances found in this study (50–10401 ind m^{-3}) were similar to those in the productive season in the South Brazilian Bight (2500–7970 ind m^{-3}; Pereira Brandini et al., 2014). The values from our study are also within the range of copepod biomass measured during November surveys of the Agulhas Bank from 1988 to 2011 (1.05 g C m^{-2} on average, J. Huggett pers. comm.; see Huggett, 2003). On average over the whole survey area, copepods comprised 65% (ranging from 5 to 97%) of the total mesozooplankton biomass in terms of carbon, while Verheye et al. (1994) estimated copepod relative abundance to be about 90%. The highest copepod biomass measured in the inner-shelf and on the wCAB (≥4 g C m^{-2}; >4000 copepods m^{-3}; >75 mg DW m^{-3}) are even comparable to some upwelling systems, for example, 3.05 g C m^{-2} in the Benguela Upwelling (southern region) in summer (Huggett et al., 2009); >70 mg DW m^{-3} and 761 ind m^{-3} for the Chilean coastal upwelling (Escribano et al., 2012; Hidalgo et al., 2010, respectively); 3–4 g C m^{-2} in the north-west of Spain (Valdes et al., 1990); 0.8–3.5 g C m^{-2} in north California (Mackas et al., 1991), and up to 2.4 g C m^{-2} in the north-west Pacific (Peterson and Keister, 2002). Hence, overall, the mesozooplankton and copepod biomass on the Agulhas Bank in autumn seems to be similar to other shelf systems, though the densities in some areas of the Agulhas Bank are more similar to productive upwelling conditions.

Within the seasonal context, the values we observed in March (early autumn) are similar to the general distribution of copepods from 24 surveys carried out in November (late spring – early summer) from 1988 to 2011 (Huggett, 2003). We can thus question whether the mesozooplankton abundances we observed are typical and correspond to a peak in productivity in autumn. On the CAB, despite the high variability in the values reported, *C. agulhensis* seemed to peak from August to November (end of winter to spring (two-year survey); De Decker et al., 1991) while on the west Agulhas Bank (Southern Benguela system), the highest zooplankton biomass was observed between February to April (end of summer to beginning of autumn; Verheye et al., 1994). Based on a 21-year climatology (remote sensing data), the highest NPP rates and Chl *a* concentrations are typically found from January to March (summer to early autumn) with a second peak of Chl *a* from July to September (end of winter to beginning of spring) (Demarcq et al., 2008; Mazwane et al., this issue). This seasonal cycle is, however, of weak magnitude with relatively high values found in winter compared to other shelf seas. The presence of phytoplankton the whole year round could partly explain why copepod egg production showed similar values in winter and summer (Huggett, 2003). Considering the lack of published zooplankton data and inter-annual variability, it is difficult to conclude whether mesozooplankton on the Agulhas Bank has a clear seasonality pattern and whether the concentrations found here in autumn correspond to a peak in productivity.

4.2. Inshore productive grounds

The clear differences in mesozooplankton densities and communities found between the inner- and outer-shelf have been observed in other shelf seas (Li et al., 2012; Mackas and Coyle, 2005; Marcolin et al., 2013;

Pereira Brandini et al., 2014; Sourisseau and Carlotti, 2006; Vandromme et al., 2014; Zhu et al., 2009). On the Agulhas Bank and on the shelf further north along the South African coast, mussel and fish larvae showed a similar trend (Beckley and Van Ballegooyen, 1992; Weidberg et al., 2015). In this study, the inshore mesozooplankton community composition was different from the outer-shelf due to a higher proportion of small taxa (*e.g.*, Calanoida, Oithonidae, Appendicularia) compared to larger mesozooplankton groups. High biomass, together with steep NBSS slopes, has been observed in other inshore environments (Marcolin et al., 2013; Vandromme et al., 2014) and can be associated with productive ecosystems dominated by herbivorous zooplankton organisms, usually smaller in size compared to carnivorous species. Alternatively, it can also be related to an increase in juvenile organisms due to enhanced reproduction stimulated by food availability (García-Comas et al., 2014; Giering et al., 2018; Mackas and Coyle, 2005; Zhou, 2006; Zhou and Huntley, 1997).

While NPP and integrated Chl *a* did not differ significantly between the inshore and offshore stations during the cruise (Poulton et al., this issue), long-term trends based on satellite data showed that the highest NPP are often observed in the inshore waters of the Agulhas Bank, partly fuelled by local coastal wind-driven upwelling (Demarcq et al., 2008, Mazwane et al., this issue). *In situ* Chl *a* measurements from previous studies have also detected inshore maxima (Probyn et al., 1994). Enhanced food availability for mesozooplankton could thus explain the higher abundance and biovolume, as well as the NBSS parameters measured during our survey. The mismatch between phytoplankton and mesozooplankton distributions during this cruise can likely be attributed to differences in the response time of these two compartments, with phytoplankton being able to adapt to changing environmental factors within a day or two.

The accumulation of biomass at the inshore stations of the Agulhas Bank might also be linked to retention mechanisms due to coastal (re-) circulation patterns and diel or ontogenic vertical migration behaviour of zooplankton (Huggett and Richardson, 2000; Peterson, 1998; Weidberg et al., 2015). Unfortunately, the lack of current data during this cruise did not allow us to investigate the influence of the inshore currents although previous studies have shown that currents on the inner bank are relatively slow, especially on the west CAB (Boyd and Shillington, 1994; Jackson et al., 2012). Along the Tsitsikamma coast, between ~23.5°E and 24.5°E (transects 7 and 8), where high mesozooplankton biomasses were observed, strong coastal wind-driven upwelling has been observed with eastward coastal currents (Boyd and Shillington, 1994; Roberts and van den Berg, 2005) which may imply recirculation and therefore possible accumulation of organisms here.

4.3. Influence of the Agulhas Current

The low abundance and shallow NBSS slopes observed at the outer-shelf stations are typical of a more oceanic environment, influenced by the warm oligotrophic Agulhas Current that flows a few nautical miles away, parallel to the shelf break. This interpretation agrees with other regions where less productive waters support less biomass and a better trophic transfer efficiency within the food web, as indicated by the shallow slopes (Marcolin et al., 2013; Vandromme et al., 2014; Zhou, 2006). The higher proportion of large mesozooplankton compared to small taxa on the outer-shelf could be attributed to a greater proportion of large carnivores (Mackas and Coyle, 2005). Moreover, larger gelatinous organisms (taxa medusae) were relatively more frequent at the outer-shelf stations than inshore (Fig. 5 and Supplementary Fig. 4), further driving shallow NBSS slopes. Finally, part of the large biovolume on the outer-shelf was also due to the high biovolume of large Calanoida. *Calanus agulhensis* developmental stages revealed an inshore-offshore long-term trend with older stages further offshore and westward, though the reason for this is still under discussion (J. Huggett pers. comm.). Overall, however, it seems that the inner- and outer bank mesozooplankton communities differ from each other due mostly to the high biovolume in the small size bins of the NBSS at the inshore stations rather than a change within the large size bins (Supplementary Fig. 4).

We observed the most distinct offshore communities (based on size diversity and community composition) on transect 7 and 6 (stations 6.3 and 7.3–7.6) which may indicate the influence of the Agulhas Current. The Agulhas Current interacts extensively with the ecosystem of the Bank through shelf-break upwelling as well as meanders and eddies formed on its inshore side and propagating south-westwards (Lutjeharms, 1981; Lutjeharms et al., 1989). Previous work has discussed how these meanders contribute to the uplift of nutrient enriched waters into the euphotic zone (Goschen et al., 2015; Jackson et al., 2012; Lutjeharms et al., 1989, 2003; Malan et al., 2018). We hypothesise that the high biomass and the different taxa composition at the stations offshore of 7.3 are a consequence of one of these meanders. Transect 7 had high Chl *a* concentration, a well-defined doming of the isotherms with slightly cooler surface temperatures at stations 7.3 and 7.4 (Fig. 2; see also Fig. 2b in Poulton et al., this issue), a relatively high concentration of upper ocean nitrate (see Fig. 3c in Poulton et al., this issue) and a low particulate load at stations 7.3 to 7.6 (*i.e.*, clear waters, see Fig. 5 in Giering et al., this issue). These elements suggest that cold, nutrient-enriched waters were present in the upper water column at the time of sampling. Remote sensing of sea level anomalies showed a relatively stable Agulhas Current flowing along the shelf break with meanders on its inshore edge (Supplementary Fig. 3a). Whether these meanders were intense enough to trigger upwelling of nutrient rich water to the surface has, however, not been proven. Having said that, an intrusion of low Chl *a* concentration filament was observed in the surface waters crossing transect 6 (Modis), most likely indicating disturbances triggered by a meander (Supplementary Fig. 3b). Another indicator of disturbance is the low NBSS linear fit at station 7.3 (r^2 = 0.26), often called a "dome" in the size spectrum theory (Quinones et al., 2003; Sourisseau and Carlotti, 2006; Zhou, 2006). This dome was caused by a high biovolume of large Euphausiacea that might indicate an advection phenomenon as described here or the sudden passage of active swimmers. Though the latter could be linked to diel vertical migration as this station was sampled at night, we consider this unlikely as our net tows sampled the entire water column (hence catching migrators regardless of their location in the water column) and we did not observe systematic differences between daytime and night-time samples (see Section 2.4). Station 6.3 is similar in composition and size diversity index to stations 7.4 and 7.5 (Figs. 4–6). While it is possible that this station was influenced by the same meander and therefore experienced similar ecosystem disturbances to the offshore stations on transect 7, a direct link is difficult to establish without an extensive analysis of the currents at the time of our survey. However, this is outside the scope of this study.

Another explanation for the mesozooplankton composition at these stations is linked to the advection of waters from the east. It has been suggested that cold water on the Agulhas Bank can originate from water being upwelled east of 26°E, often referred to as the "Port Alfred" upwelling, which then moves westwards on the shelf (Largier and Swart, 1987; Lutjeharms, 2006; Swart and Largier, 1987). High surface remotely sensed Chl *a* concentrations were observed in that region on 16–17 March 2019, nine days prior to the cruise (data not shown). Assuming a westward current speed of approximately 0.2 m s^{-1} (L. Hancke, pers. comm.), this Chl *a* enriched water could have reached transect 7 in about 10–15 days (~180–265 km), which is when sampling was conducted. Hence localised upwelling or advection of waters from the east could explain the presence of an atypical mesozooplankton community at the offshore stations of transect 7.

4.4. Longitudinal differences in mesozooplankton community

The second noticeable trend in the mesozooplankton community on the Agulhas Bank was the longitudinal differences with three distinct zones: the far east of the Agulhas Bank (off Port Alfred), the central part

of the Bank (wEAB and eCAB, between 22 and 26°E) and the far west of the CAB (west of 22°E).

The coast between Port Alfred and Algoa Bay has been identified in the literature as an upwelling centre stimulating production (Goschen et al., 2012; Goschen and Schumann, 1988; Mazwane et al., this issue). The hydrographic and nutrient profiles show that the upwelling was not active at the time of sampling. Chl *a* concentration was, however, relatively high, especially at station 1.1, while NPP was relatively low (Poulton et al., this issue). Giering et al. (this issue) highlighted the presence of large (>100 μm) Chl *a* rich aggregates or phytoplankton cells and suggested that these indicate the end of an upwelling event. The low mesozooplankton biovolume, as well as the size characteristic of the community (steep slope and low size diversity), suggest a short food web with low trophic transfer efficiency. Yet the high linear fit of the NBSS highlights a steady environment without any perturbation which is often observed in stable environments (e.g., no blooms) such as oligotrophic systems (reviewed by Sprules and Barth, 2015). Finally, the spAARS activity was average, suggesting that the mesozooplankton was not responding to a pulse of phytoplankton or that the food was unavailable to the mesozooplankton community (*e.g.*, not the right size or species). The Port Alfred upwelling might be too short-lived or the environment too turbulent (*i.e.*, narrow shelf strongly influenced by the Agulhas Current) to be able to see a mesozooplankton response at that location.

The wEAB and eCAB were similar in terms of mesozooplankton taxa composition, integrated biovolumes and size structure, indicating that these regions are relatively well connected and experience similar drivers, of which the distance to the coast might be the dominant one.

Finally, the wCAB (inner-shelf of transect 11 and 12) was clearly distinguishable from the other stations. This region was characterized by deeper MLD, low NPP (Fig. 5e), high integrated Chl *a* and deep (>30 m) Chl *a* maximum, as well as low dissolved oxygen below the upper mixed layer (see Giering et al., this issue). Giering et al. (this issue) proposed that this low dissolved oxygen could be the result of accumulated remineralisation caused by the presence of a retention area with low current speed and a cyclonic circulation (Boyd et al., 1992; Boyd and Shillington, 1994). Poulton et al. (this issue) also highlighted high nitrate to phosphate concentrations in the bottom waters of that area, a potential signal of sedimentary denitrification in the retention area. At these stations, the elevated biomass of doliolids and Calanoida copepods found during our survey may also have contributed to this low dissolved oxygen zone by additional respiration and/or production of particles (*e.g.*, carcasses, sloppy feedings, faecal pellets) which are an organic rich habitat for bacteria and other organisms (Frischer et al., 2021; Thor et al., 2003). Doliolids are known for their asexual and sexual reproduction modes which enable them to rapidly 'bloom', reaching high concentrations in a short period of time when food conditions are favourable (Ishak et al., 2020; Martin et al., 2017; Paffenhöfer and Köster, 2005; Takahashi et al., 2015; Walters et al., 2019). Hence the increase in food availability (high integrated Chl *a*), coupled with the recirculation, might favour enhanced Calanoida and doliolid biomass and resulted in the steep NBSS slopes on the wCAB.

On the CAB along the 100 m isobath, high copepod biomass has previously been reported and linked to the presence of a 'Cold Ridge' (Peterson and Hutchings, 1995). This was largely based on a few cruises, especially the ones from 1988 to 1989 when high concentrations of zooplankton were reported over the whole Bank (~2 g C m^{-2}, assuming a 40% of carbon to dry weight ratio). Later, with 24 cruises from 1988 to 2011, Huggett (2003) confirmed that copepod biomasses are high along the 100 m isobath on the CAB, mostly driven by the large calanoid *C. agulhensis*. During our study, we did not observe a Cold Ridge, yet copepods were extremely abundant in this region (max = 4 g C m^{-2}). Our data suggest that zooplankton biomass can be high in this region with or without the presence of a marked dome of cold water. We hypothesise that the high biomass of zooplankton observed on the wCAB was not linked to any specific upwelled water but rather due to a less dynamic environment which allows concentration and retention of biomass with greater remineralisation than the rest of the Bank. Other mixing mechanisms, such as internal tides or wind, can also be at the origin of increased production in this area, contributing to the diffusion of nutrient in the surface layer (Jackson et al., 2012; Largier and Swart, 1987).

4.5. Mesozooplankton production and trophic transfer efficiency on the Agulhas Bank

The spAARS activity of zooplankton on the Agulhas Bank (90.8 ± 0.6 nmol PPi hr^{-1} mg $prot^{-1}$) was lower than measurements from Northwest Australia (~140 nmol PPi hr^{-1} mg $prot^{-1}$ for size fraction >150 μm) while ZP estimates were similar (~0.28 g C m^{-2} d^{-1}, McKinnon et al., 2015, Table 2). Our values were also in the same range as previous estimates made by Peterson and Hutchings (1995) on the Agulhas Bank (0.04–0.4 g C m^{-2} d^{-1}) and in the Alboran coastal waters (South-West Mediterranean Sea) (0.18 mg C m^{-2} d^{-1}, Yebra et al., 2017b), which were much higher than previous studies of the same region (0.0006–0.06 mg C m^{-2} d^{-1}, Yebra et al., 2017b and references within). It is worth noting that, due to the vertical nets used during our cruise, the biomass and production were integrated over the whole water column. In the calculation of the ZP (using the Arrhenius equation), we thus used an average *in situ* temperature (Yebra et al., 2017a). Due to the strong stratification on the Bank (>18°C in surface waters, 10°C in deep waters), these average temperatures tended to be relatively low (average of 12.8°C) compared to upper ocean waters (closer to 20°C). Zooplankton perform diel vertical migration, so it is most likely that they spend time above and below the thermocline. This behaviour is well described for *C. agulhensis*, one of the dominant copepods on the Bank (Huggett and Richardson, 2000). If zooplankton spent more time in the upper layer, it is possible that the ZP estimations presented here are slightly underestimated (average value of ~0.45 g C m^{-2} d^{-1} when SST is used which is ~1.5 times higher than we presented).

Overall, spAARS did not vary much over the survey area and only transect 6 (and 7 and 8 to a lesser extent) showed high spAARS values, which, as hypothesised above, could be linked to a local upwelling or horizontal advection of water. Hence biomass was the main driver of the distribution of ZP on the Agulhas Bank, as in other studies (Garijo and Hernández-León, 2015 and references within). The lack of correlation between ZP and integrated Chl *a* or NPP suggests that phytoplankton was not the main driver of the distribution of ZP. The trophic transfer efficiency represented here by plotting NPP (Poulton et al., this issue) against ZP (Fig. 9), both measured simultaneously during the cruise, was variable, with a set of values sitting along the 30% and 100% efficiency, while other values were far above the 1:1 line. Most of the stations with 30% efficiency were on the EAB and outer- and mid-shelf of the eCAB. This value agrees with previous estimations whereby copepods would consume 20% (*C. agulhensis* and small copepods only; Peterson and Hutchings, 1995) or 30–50% (based on a 100% phytoplankton diet; Verheye et al., 1994) of the daily primary production. The higher efficiency values (~100%) are mainly found at stations sampled on the inner- and mid-shelf of the CAB where high biovolumes were found.

Some methodological aspects need to be considered when interpreting these data. The mesozooplankton were not size-fractionated prior to measurement of their enzymatic activity, hence the ZP estimates represent the whole community, including non-herbivorous species which do not rely on photosynthetic organisms as prey. The Agulhas Bank had a relatively low number of diatoms (Poulton et al., this issue), suggesting that trophic energy was also channelled via microzooplankton which was not estimated during this cruise. Despite these methodological considerations and considering that microzooplankton have an important grazing impact on phytoplankton (Armengol et al., 2019), our data suggest that the mesozooplankton on the Agulhas Bank may be food-limited which is in agreement with the conclusion of Peterson and Hutchings (1995). This conclusion, however, contradicts

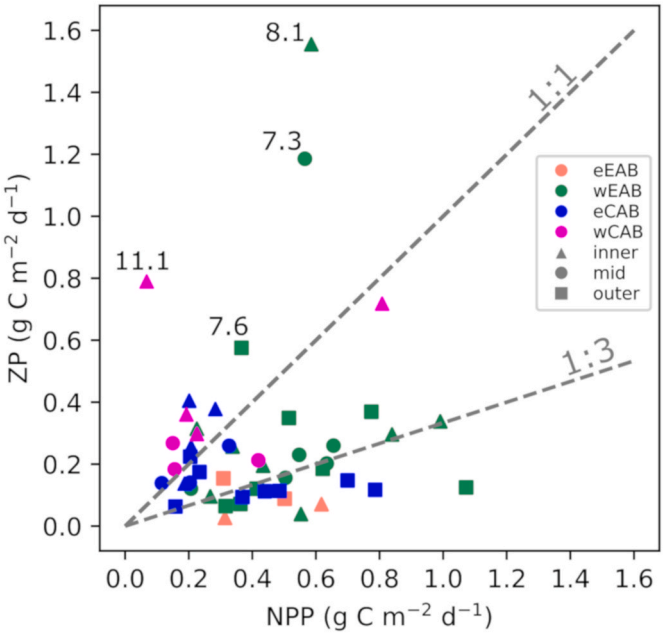

Fig. 9. Scatterplot of the mesozooplankton production (ZP, in g C m^{-2} d^{-1}) against Net Primary Production (NPP in g C m^{-2} d^{-1} from Poulton et al., this issue) coded according to the zones studied (see legend: eEAB, eastern East Agulhas Bank; wEAB, western East Agulhas Bank; eCAB: eastern Central Agulhas Bank; wCAB: western Central Agulhas Bank; inner-mid-outer-shelf). The two grey dotted lines represent the 1:1 and 1:3 ratios. Numbers next to some symbols correspond to station number.

other studies which highlighted that trophic relationships have a stronger impact on ZP than hydrographic conditions (Yebra 2007b and references within). This discrepancy can also be due to the fact that cruises are only a snapshot of a system that is often far from steady-state, and even more so in the case of the highly dynamic Agulhas Bank.

Four stations showed a drastic difference between ZP and NPP: stations 7.3, 7.6, 8.1 and 11.1, all of which had high biomass, high ZP and low NPP (Fig. 9). The two stations on transect 7 were, as discussed above, most likely influenced by a local upwelling or advection. At station 8.1, chaetognaths, large calanoids and Euphausiacea represented 77.5% of the total carbon biomass. This station was also characterised by high bottom turbidity, low particle load in the MLD (Giering et al., this issue), a deep euphotic zone (Poulton et al., this issue) and average integrated Chl *a* concentration. As discussed before, this section of the coast is subject to wind-driven coastal upwelling, and surface remotely sensed Chl *a* concentrations were relatively high 10 days prior to the cruise. The high mesozooplankton biomass we observed might be in response to that past event. Station 11.1 had a high biomass of large Calanoida (64% of the total carbon), an above average ZP, but more striking was the very low NPP with a sub-surface Chl *a* maximum at 32 m, most likely due to photo-acclimated deep phytoplankton (Poulton et al., this issue). The overall integrated Chl *a* concentration was, however, relatively high and might have contributed to sustain the high mesozooplankton density. The strong imbalance between carbon demand (ZP) and carbon supply (NPP) is most likely due to the dynamic nature at these stations, the complex marine trophic relationships and the fact that primary and secondary producers have different time responses. Snapshot measurements, like those from short cruises, cannot always resolve such complex relationships.

It is interesting to note that steep NBSS slopes, which imply a higher proportion of small organisms compared to large ones, were not correlated to ZP or spAARS ($p > 0.05$, $n = 47$). One could have expected higher spAARS in a system dominated by small-sized organisms (including juveniles) due to their higher metabolic rates (Brown et al., 2004). This lack of correlation may be due to the fact that the enzymatic assay was done on the whole mesozooplankton community and that somatic growth may not be as sensitive to environmental changes as other physiological parameters. For instance, reproduction is more sensitive to food availability than growth (Kiørboe, 1998). The negative relationship between NBSS slopes and intercepts contradicts the size spectrum theory whereby shallow NBSS slopes would usually lead to higher biomass due to better transfer efficiency between trophic levels (reviewed by Sprules and Barth, 2015). In the literature, however, positive and negative relationships between these two parameters have been found, meaning that steep slopes are found in both oligotrophic and productive ecosystems (*e.g.*, Giering et al., 2018; Marcolin et al., 2013; Noyon et al., 2020; San Martin et al., 2006; Vandromme et al., 2014; Zhou et al., 2009; Zhou and Huntley, 1997). As suggested by Marcolin et al. (2013), it is important to take into consideration the size range used to compute a NBSS. For instance, Giering et al. (2018) found a positive correlation between the NBSS slopes and intercepts, but phytoplankton were included in the NBSS and the study was over three seasons. Over the spring productive season, however, they found a steep zooplankton NBSS slope which they interpreted as a response of the zooplankton to the spring bloom (Giering et al., 2018) which is similar to our interpretation on the inner bank. It is thus important to consider the ecosystem's overall context at the time of sampling when interpreting NBSS parameters.

4.6. *Concluding remarks and implications for ecosystem productivity*

This study highlighted a clear inshore-offshore gradient with a higher abundance and biovolume of mesozooplankton in the inshore waters, together with a larger proportion of small organisms compared to large ones. Mesozooplankton, including large calanoids, seem to accumulate on the inner-shelf of the CAB, most likely due to the local circulation and the possible presence of a retention cell, which is partly fuelled by organic matter remineralisation processes, which requires additional focused investigation. On the EAB and CAB in autumn, the mesozooplankton biomass and production was, overall, in the same range as other continental shelf seas, and the CAB was even comparable to upwelling regions. This relatively high mesozooplankton biomass may be caused by the distinct hydrography and seasonal cycle in primary production. Compared to other shelf seas, the Agulhas Bank is characterised by an intense thermocline, partly caused by shelf-edge upwelling, advecting Indian Ocean Central Water onto the shelf (Boyd and Shillington, 1994; Jackson et al., 2012; Swart and Largier, 1987). The cold nutrient-enriched bottom water is available throughout the year and can fuel primary production in the sunlit layer, depending on the thermocline dynamics (e.g., mixing, vertical diffusion; Poulton et al., this issue). This may explain the weak magnitude of the primary production seasonal cycle on the Agulhas Bank (Demarcq et al., 2008; Mazwane et al., this issue), which can provide a relatively constant source of prey for zooplankton communities. Overall, the nutrient supply processes operating on the CAB and EAB may work very differently from other shelf seas of similar latitudes and require further investigation, especially during the winter when stratification might still exist. It has also been suggested that the high biomass of copepods on the CAB and EAB could be a consequence of reduced predation pressure from fish, which are less abundant there compared to the west coast of South Africa (Peterson et al., 1992; Verheye et al., 1994).

Author contributions

Margaux Noyon: Conceptualization, Data curation, Formal analysis, Investigation, Visualization, Writing - original draft, Writing - review and editing; **Alex J. Poulton**: Funding acquisition, Investigation, Formal analysis, Writing - original draft, Writing – review and editing; **Sarah Asdar**: Methodology, Visualization, Formal analysis, Writing – review and editing; **Riaan Weitz**: Data curation; **Sarah L. C. Giering**:

Conceptualization, Investigation, Writing - original draft, Writing – review and editing.

Declaration of competing interest

The authors declare that they have no known competing financial interests or personal relationships that could have appeared to influence the work reported in this paper.

Acknowledgements

We thank the captain and crew of the RV *Ellen Kuzwayo,* as well as the Department of Agriculture, Forestry and Fisheries (now DFFE). Thank you to Lidia Yebra and Kathryn Cook for their advice on the AARS method. We would also like to thank the South African Environmental Observation Network (SAEON), a business unit of the National Research Foundation (NRF), supported by the Shallow Marine and Coastal Research Infrastructure (SMCRI) initiative of the Department of Science and Innovation (DSI), for the use of their ZooScan. We are also thankful to the scientists of the SOLSTICE-WIO project for fruitful discussions. This publication was produced with the financial support of the Global Challenges Research Fund (GCRF), UK, in the framework of the SOLSTICE-WIO project [NE/P021050/1]. This work is also part of the UK-SA Bilateral Chair in Ocean Science and Marine Food Security funded by the British Council Newton Fund grant SARCI 1503261 16102/NRF 98399.

Appendix A. Supplementary data

Supplementary data to this article can be found online at https://doi.org/10.1016/j.dsr2.2021.105015.

References

Andersen, K.H., Berge, T., Gonçalves, R.J., Hartvig, M., Heuschele, J., Hylander, S., Jacobsen, N.S., Lindemann, C., Martens, E.A., Neuheimer, A.B., Olsson, K., Palacz, A., Prowe, A.E.F., Sainmont, J., Traving, S.J., Visser, A.W., Wadhwa, N., Kiørboe, T., 2016. Characteristic sizes of life in the oceans, from bacteria to whales. Ann. Rev. Mar. Sci 8, 217–241. https://doi.org/10.1146/annurev-marine-122414-034144.

Armengol, L., Calbet, A., Franchy, G., Rodríguez-Santos, A., Hernández-León, S., 2019. Planktonic food web structure and trophic transfer efficiency along a productivity gradient in the tropical and subtropical Atlantic Ocean. Sci. Rep. 9, 2044. https://doi.org/10.1038/s41598-019-38507-9.

Basedow, S.L., Tande, K.S., Zhou, M., 2010. Biovolume spectrum theories applied: spatial patterns of trophic levels within a mesozooplankton community at the polar front. J. Plankton Res. 32, 1105–1119. https://doi.org/10.1093/plankt/fbp110.

Bauer, J.E., Cai, W.-J., Raymond, P.A., Bianchi, T.S., Hopkinson, C.S., Regnier, P.A.G., 2013. The changing carbon cycle of the coastal ocean. Nature 504, 61–70. https://doi.org/10.1038/nature12857.

Beckley, L.E., Van Ballegooyen, R.C., 1992. Oceanographic conditions during three ichthyoplankton surveys of the Agulhas Current in 1990/91. S. Afr. J. Mar. Sci. 12, 83–93. https://doi.org/10.2989/02577619209504693.

Bianchi, G., Skjoldal, H.R., 2008. The Ecosystem Approach to Fisheries. FAO- CABI, Oxfordshire, p. 363pp.

Boyd, A.J., Shillington, F.A., 1994. Physical forcing and circulation patterns on the Agulhas Bank. South Afr. J. Sci. 90, 143–154. https://doi.org/10.10520/AJA00382353_4624.

Boyd, A.J., Taunton-Clark, J., Oberholster, G.P.J., 1992. Spatial features of the near-surface and midwater circulation patterns off western and southern South Africa and their role in the life histories of various commercially fished species. S. Afr. J. Mar. Sci. 12, 189–206. https://doi.org/10.2989/02577619209504702.

Brown, J.H., Gillooly, J.F., Allen, A.P., Savage, V.M., West, G.B., 2004. Toward a metabolic theory of ecology. Ecology 1771–1789. https://doi.org/10.1890/03-9000@10.1002/(ISSN)1939-9170. MacArthurAward.

Carvalho, F., Kohut, J., Oliver, M.J., Schofield, O., 2017. Defining the ecologically relevant mixed-layer depth for Antarctica's coastal seas. Geophys. Res. Lett. 44, 338–345. https://doi.org/10.1002/2016GL071205.

Dai, L., Li, C., Yang, G., Sun, X., 2016. Zooplankton abundance, biovolume and size spectra at western boundary currents in the subtropical North Pacific during winter 2012. J. Mar. Syst. 155, 73–83. https://doi.org/10.1016/j.jmarsys.2015.11.004.

De Decker, A., Kaczmaruk, B., Marska, G., 1991. A new species of Calanus (Copepoda, Calanoida) from South African waters. Ann. S. Afr. Mus. 101, 27–44.

Demarcq, H., Richardson, A.J., Field, J.G., 2008. Generalised model of primary production in the southern Benguela upwelling system. Mar. Ecol. Prog. Ser. 354, 59–74. https://doi.org/10.3354/meps07136.

Escribano, R., Hidalgo, P., Fuentes, M., Donoso, K., 2012. Zooplankton time series in the coastal zone off Chile: variation in upwelling and responses of the copepod community. Prog. Oceanogr., Series 97–100, 174–186. https://doi.org/10.1016/j.pocean.2011.11.006.

Frischer, M.E., Lamboley, L.M., Walters, T.L., Brandes, J.A., Arneson, E., Lacy, L.E., López-Figueroa, N.B., Rodríguez-Santiago, Á.E., Gibson, D.M., 2021. Selective feeding and linkages to the microbial food web by the doliolid Dolioletta gegenbauri. Limnol. Oceanogr. n/a. https://doi.org/10.1002/lno.11740.

García-Comas, C., Chang, C.-Y., Ye, L., Sastri, A.R., Lee, Y.-C., Gong, G.-C., Hsieh, C., 2014. Mesozooplankton size structure in response to environmental conditions in the East China Sea: how much does size spectra theory fit empirical data of a dynamic coastal area? Prog. Oceanogr. 121, 141–157. https://doi.org/10.1016/j.pocean.2013.10.010.

Garijo, J.C., Hernández-León, S., 2015. The use of an image-based approach for the assessment of zooplankton physiological rates: a comparison with enzymatic methods. J. Plankton Res. 37, 923–938. https://doi.org/10.1093/plankt/fbv056.

Giering, S., Noyon, M., Godfrey, B., Poulton, A.J., Briggs, N., Roberts, M. This issue. Optical particle measurements indicate resuspension as dominant mechanisms behind the formation of benthic nepheloid layers on the Agulhas Bank. Deep Sea Res. Part II Top. Stud. Oceanogr.

Giering, S.L.C., Wells, S.R., Mayers, K.M.J., Schuster, H., Cornwell, L., Fileman, E.S., Atkinson, A., Cook, K.B., Preece, C., Mayor, D.J., 2018. Seasonal variation of zooplankton community structure and trophic position in the Celtic Sea: a stable isotope and biovolume spectrum approach. Prog. Oceanogr. https://doi.org/10.1016/j.pocean.2018.03.012.

Gillooly, J.F., Brown, J.H., West, G.B., Savage, V.M., Charnov, E.L., 2001. Effects of size and temperature on metabolic rate. Science 293, 2248–2251. https://doi.org/10.1126/science.1061967.

Gorsky, G., Ohman, M.D., Picheral, M., Gasparini, S., Stemmann, L., Romagnan, J.-B., Cawood, A., Pesant, S., García-Comas, C., Prejger, F., 2010. Digital zooplankton image analysis using the ZooScan integrated system. J. Plankton Res. 32, 285–303. https://doi.org/10.1093/plankt/fbp124.

Goschen, W.S., Bornman, T.G., Deyzel, S.H.P., Schumann, E.H., 2015. Coastal upwelling on the far eastern Agulhas Bank associated with large meanders in the Agulhas Current. Continent. Shelf Res. 101, 34–46. https://doi.org/10.1016/j.csr.2015.04.004.

Goschen, W.S., Schumann, E.H., 1990. Agulhas current variability and inshore structures off the Cape Province, South Africa. J. Geophys. Res. Oceans 95, 667–678. https://doi.org/10.1029/JC095iC01p00667.

Goschen, W.S., Schumann, E.H., 1988. Ocean current and temperature structures in Algoa Bay and beyond in November 1986. South Afr. J. Mar. Sci. 7, 101–116. https://doi.org/10.2989/025776188784379198.

Goschen, W.S., Schumann, E.H., Bernard, K.S., Bailey, S.E., Deyzel, S.H.P., 2012. Upwelling and ocean structures off Algoa Bay and the south-east coast of South Africa. Afr. J. Mar. Sci. 34, 525–536. https://doi.org/10.2989/1814232X.2012.749810.

Hidalgo, P., Escribano, R., Vergara, O., Jorquera, E., Donoso, K., Mendoza, P., 2010. Patterns of copepod diversity in the Chilean coastal upwelling system. Deep Sea Res. Part II Top. Stud. Oceanogr. 57, 2089–2097. https://doi.org/10.1016/j.dsr2.2010.09.012.

Hirst, A.G., Roff, J.C., Lampitt, R.S., 2003. A synthesis of growth rates in marine epipelagic invertebrate zooplankton. In: Southward, A.J., Tyler, P.A., Young, C.M., Fuiman, L.A. (Eds.), Advances in Marine Biology. Academic Press, pp. 1–142. https://doi.org/10.1016/S0065-2881(03)44002-9.

Hopkins, J., Palmer, M., Poulton, A.J., Hickman, A.E., Sharples, J., 2021. Control of a phytoplankton bloom by wind-driven vertical mixing and light availability. Limnol. Oceanogr. 66 (5), 1926–1949. https://doi.org/10.1002/lno.11734.

Huggett, J., Verheye, H., Escribano, R., Fairweather, T., 2009. Copepod biomass, size composition and production in the Southern Benguela: spatio–temporal patterns of variation, and comparison with other eastern boundary upwelling systems. Prog. Oceanogr. 83, 197–207. https://doi.org/10.1016/j.pocean.2009.07.048.

Huggett, J.A., 2003. Comparative Ecology of the Copepods Calanoides Carinatus and calanus Agulhensis in the Southern Benguela and Agulhas Bank Ecosystems. PhD thesis. University of Cape, Town, p. 296.

Huggett, J.A., Richardson, A.J., 2000. A review of the biology and ecology of Calanus agulhensis off South Africa. ICES J. Mar. Sci. 57, 1834–1849. https://doi.org/10.1006/jmsc.2000.0977.

Hutchings, L., Beckley, L., Griffiths, M., Roberts, M., Sundby, S., van der Lingen, C., 2002. Spawning on the edge: spawning grounds and nursery areas around the southern African coastline. Mar. Freshw. Res. 53, 307–318. https://doi.org/10.1071/MF01147.

Hutchings, L., Verheye, H.M., Mitchell-Innes, B.A., Peterson, W.T., Huggett, J.A., Painting, S.J., 1995. Copepod production in the southern Benguela system. ICES J. Mar. Sci. 52, 439–455. https://doi.org/10.1016/1054-3139(95)80059-X.

Ishak, N.H.A., Tadokoro, K., Okazaki, Y., Kakehi, S., Suyama, S., Takahashi, K., 2020. Distribution, biomass, and species composition of salps and doliolids in the Oyashio–Kuroshio transitional region: potential impact of massive bloom on the pelagic food web. J. Oceanogr. 76, 351–363. https://doi.org/10.1007/s10872-020-00549-3.

Jackson, J.M., Rainville, L., Roberts, M.J., McQuaid, C.D., Lutjeharms, J.R.E., 2012. Mesoscale bio-physical interactions between the Agulhas current and the Agulhas Bank, South Africa. Continent. Shelf Res. 49, 10–24. https://doi.org/10.1016/j.csr.2012.09.005.

Keister, J.E., Peterson, W.T., Pierce, S.D., 2009. Zooplankton distribution and cross-shelf transfer of carbon in an area of complex mesoscale circulation in the northern

California Current. Deep-Sea Res. Part A Oceanogr. Res. Pap. 56, 212–231. https://doi.org/10.1016/j.dsr.2008.09.004.
Kiørboe, T., 2016. Foraging mode and prey size spectra of suspension-feeding copepods and other zooplankton. Mar. Ecol. Prog. Ser. 558, 15–20. https://doi.org/10.3354/meps11877.
Kiørboe, T., 2013. Zooplankton body composition. Limnol. Oceanogr. 58, 1843–1850. https://doi.org/10.4319/lo.2013.58.5.1843.
Kiørboe, T., 1998. Population regulation and role of mesozooplankton in shaping marine pelagic food webs. In: Tamminen, T., Kuosa, H. (Eds.), Eutrophication in Planktonic Ecosystems: Food Web Dynamics and Elemental Cycling. Springer Netherlands, Dordrecht, pp. 13–27. https://doi.org/10.1007/978-94-017-1493-8_2.
Kiørboe, T., Hirst, A.G., 2014. Shifts in mass scaling of respiration, feeding, and growth rates across life-Form transitions in marine pelagic organisms. Am. Nat. 183, E118–E130. https://doi.org/10.1086/675241.
Largier, J.L., Swart, V.P., 1987. East-west variation in thermocline breakdown on the Agulhas Bank. South Afr. J. Mar. Sci. 5, 263–272. https://doi.org/10.2989/025776187784522252.
Lehette, P., Hernández-León, S., 2009. Zooplankton biomass estimation from digitized images: a comparison between subtropical and Antarctic organisms. Limnol Oceanogr. Methods 7, 304–308. https://doi.org/10.4319/lom.2009.7.304.
Li, K., Yin, J., Huang, L., Lian, S., Zhang, J., 2012. Distribution patterns of appendicularians and copepods and their relationship on the northwest continental shelf of South China Sea during summer. Acta Oceanol. Sin. 31, 135–145. https://doi.org/10.1007/s13131-012-0243-7.
Lowry, O.H., Rosebrough, N.J., Farr, A.L., Randall, R.J., 1951. Protein measurement with the Folin phenol reagent. J. Biol. Chem. 193, 265–275.
Lutjeharms, J., 2006. The Agulhas Current. Springer-Verlag, Berlin Heidelberg. https://doi.org/10.1007/3-540-37212-1.
Lutjeharms, J.R.E., 1981. Features of the Southern Agulhas current circulation from satellite remote sensing. South Afr. J. Sci. 77, 231–236. https://doi.org/10.10520/AJA00382353_1526.
Lutjeharms, J.R.E., Boebel, O., Rossby, H.T., 2003. Agulhas cyclones. Deep Sea Res. Part II Top. Stud. Oceanogr. 50, 13–34. https://doi.org/10.1016/S0967-0645(02)00378-8.
Lutjeharms, J.R.E., Catzel, R., Valentine, H.R., 1989. Eddies and other boundary phenomena of the Agulhas Current. Continent. Shelf Res. 9, 597–616. https://doi.org/10.1016/0278-4343(89)90032-0.
Lutjeharms, J.R.E., Cooper, J., Roberts, M., 2000. Upwelling at the inshore edge of the Agulhas current. Continent. Shelf Res. 20, 737–761. https://doi.org/10.1016/S0278-4343(99)00092-8.
Lutjeharms, J.R.E., Meyer, A.A., Ansorge, I.J., Eagle, G.A., Orren, M.J., 1996. The nutrient characteristics of the Agulhas Bank. S. Afr. J. Mar. Sci. 17, 253–274. https://doi.org/10.2989/025776196784158464.
Mackas, D.L., Coyle, K.O., 2005. Shelf–offshore exchange processes, and their effects on mesozooplankton biomass and community composition patterns in the northeast Pacific. Deep Sea Res. Part II Top. Stud. Oceanogr. 52, 707–725. https://doi.org/10.1016/j.dsr2.2004.12.020.
Mackas, D.L., Washburn, L., Smith, S.L., 1991. Zooplankton community pattern associated with a California Current cold filament. J. Geophys. Res. Oceans 96, 14781–14797. https://doi.org/10.1029/91JC01037.
Malan, N., Backeberg, B., Biastoch, A., Durgadoo, J.V., Samuelsen, A., Reason, C., Hermes, J., 2018. Agulhas current meanders facilitate shelf-slope exchange on the Eastern Agulhas Bank. J. Geophys. Res. Oceans 123, 4762–4778. https://doi.org/10.1029/2017JC013602.
Marcolin, C. da R., Schultes, S., Jackson, G.A., Lopes, R.M., 2013. Plankton and seston size spectra estimated by the LOPC and ZooScan in the Abrolhos Bank ecosystem (SE Atlantic). Continent. Shelf Res. 70, 74–87. https://doi.org/10.1016/j.csr.2013.09.022.
Martin, B., Koppelmann, R., Kassatov, P., 2017. Ecological relevance of salps and doliolids in the northern Benguela Upwelling System. J. Plankton Res. 39, 290–304. https://doi.org/10.1093/plankt/fbw095.
Mazwane, S.L., Poulton, A.J., Hickman, A., Jebri, F., Jacobs Z., Roberts, M., Noyon, M. This issue. Seasonal and long-term stability of net primary production on the Agulhas Bank, 1998 - 2018. Deep Sea Res. Part II Top. Stud. Oceanogr.
McKinnon, A.D., Doyle, J., Duggan, S., Logan, M., Lønborg, C., Brinkman, R., 2015. Zooplankton growth, respiration and grazing on the Australian margins of the tropical Indian and Pacific Oceans. PLoS One 10, e0140012. https://doi.org/10.1371/journal.pone.0140012.
Noyon, M., 2019. Ellen Khuzwayo EK188 - Cruise Summary Report. Southampton.
Noyon, M., Rasoloarijao, Z., Huggett, J., Ternon, J.-F., Roberts, M., 2020. Comparison of mesozooplankton communities at three shallow seamounts in the South West Indian Ocean. Deep Sea Res. Part II Top. Stud. Oceanogr. 176 https://doi.org/10.1016/j.dsr2.2020.104759, 104759.
Noyon, M., 2021. Mesozooplankton Imaging Analyses Including Size, Abundance, Biovolume, Biomass Estimates and Identification for the Agulhas Bank EK188 Cruise (SOLSTICE Program). NERC EDS British Oceanographic Data Centre NOC doi:10/gznf.
Oksanen, J., Blanchet, F.G., Friendly, M., Kindt, R., Legendre, P., McGlinn, D., Minchin, P.R., O'Hara, R.B., Simpson, G.L., Solymos, P., Stevens, M.H.H., Szoecs, E., Wagner, H., 2020. Vegan: community ecology package. R Package Version 2 5–7.
Paffenhöfer, G.-A., Köster, M., 2005. Digestion of diatoms by planktonic copepods and doliolids. Mar. Ecol. Prog. Ser. 297, 303–310. https://doi.org/10.3354/meps297303.
Pauly, D., Christensen, V., Guénette, S., Pitcher, T.J., Sumaila, U.R., Walters, C.J., Watson, R., Zeller, D., 2002. Towards sustainability in world fisheries. Nature 418, 689–695. https://doi.org/10.1038/nature01017.
Pereira Brandini, F., Nogueira, M., Simião, M., Carlos Ugaz Codina, J., Almeida Noernberg, M., 2014. Deep chlorophyll maximum and plankton community response to oceanic bottom intrusions on the continental shelf in the South Brazilian Bight. Continent. Shelf Res. 89, 61–75. https://doi.org/10.1016/j.csr.2013.08.002.
Peterson, W., 1998. Life cycle strategies of copepods in coastal upwelling zones. J. Mar. Syst. 15, 313–326. https://doi.org/10.1016/S0924-7963(97)00082-1.
Peterson, W.T., Hutchings, L., 1995. Distribution, abundance and production of the copepod Calanus agulhensis on the Agulhas Bank in relation to spatial variations in hydrography and chlorophyll concentration. J. Plankton Res. 17, 2275–2294. https://doi.org/10.1093/plankt/17.12.2275.
Peterson, W.T., Hutchings, L., Huggett, J.A., Largier, J.L., 1992. Anchovy spawning in relation to the biomass and the replenishment rate of their copepod prey on the western Agulhas Bank. South Afr. J. Mar. Sci. 12, 487–500. https://doi.org/10.2989/02577619209504720.
Peterson, W.T., Keister, J.E., 2002. The effect of a large cape on distribution patterns of coastal and oceanic copepods off Oregon and northern California during the 1998–1999 El Niño–La Niña. Prog. Oceanogr. 53, 389–411. https://doi.org/10.1016/S0079-6611(02)00038-1.
Picheral, M., Colin, S., Irison, J.-O., 2017. EcoTaxa, a tool for the taxonomic classification of images. http://ecotaxa.obs-vlfr.fr.
Platt, T., Denman, K., 1977. Organisation in the pelagic ecosystem. Helgol. Wiss. Meeresunters. 30, 575. https://doi.org/10.1007/BF02207862.
Poulton, A.J., Mazwane, S.L., Godfrey, B., Carvalho, A., Mawji, E., Wihsgott, J.U., Noyon, M. This issue. Primary production dynamics on the Agulhas Bank in autumn (March 2019). Deep Sea Res. Part II Top. Stud. Oceanogr.
Porri, F., Jackson, J.M., Von der Meden, C.E.O., Weidberg, N., McQuaid, C.D., 2014. The effect of mesoscale oceanographic features on the distribution of mussel larvae along the south coast of South Africa. J. Mar. Syst. 132, 162–173. https://doi.org/10.1016/j.jmarsys.2014.02.001.
Probyn, T.A., Mitchell-Innes, B.A., Brown, P.C., Hutchings, L., Carter, R.A., 1994. A review of primary production and related processes on the Agulhas-Bank. South Afr. J. Mar. Sci. 90 (3), 166–173. https://hdl.handle.net/10520/AJA00382353_4632.
Quinones, R.A., Platt, T., Rodríguez, J., 2003. Patterns of biomass-size spectra from oligotrophic waters of the Northwest Atlantic. Prog. Oceanogr. 57, 405–427. https://doi.org/10.1016/S0079-6611(03)00108-3.
Quintana, X.D., Brucet, S., Boix, D., López-Flores, R., Gascón, S., Badosa, A., Sala, J., Moreno-Amich, R., Egozcue, J.J., 2008. A nonparametric method for the measurement of size diversity with emphasis on data standardization. Limnol Oceanogr. Methods 6, 75–86. https://doi.org/10.4319/lom.2008.6.75.
Quintana, X.D., Egozcue, J.J., Martínez-Abella, O., López-Flores, R., Gascón, S., Brucet, S., Boix, D., 2016. Update: a non-parametric method for the measurement of size diversity, with emphasis on data standardization. The measurement of the size evenness. Limnol Oceanogr. Methods 14, 408–413. https://doi.org/10.1002/lom3.10099.
Roberts, M.J., van den Berg, M., 2005. Currents along the Tsitsikamma coast, South Africa, and potential transport of squid paralarvae and ichthyoplankton. Afr. J. Mar. Sci. 27, 375–388. https://doi.org/10.2989/18142320509504096.
Rodriguez, J., Mullin, M.M., 1986. Relation between biomass and body weight of plankton in a steady state oceanic ecosystem1. Limnol. Oceanogr. 31, 361–370. https://doi.org/10.4319/lo.1986.31.2.0361.
San Martin, E., Irigoien, X., Harris Roger, P., Urrutia, Â.L., Zubkov, M.V., Heywood, J.L., 2006. Variation in the transfer of energy in marine plankton along a productivity gradient in the Atlantic Ocean. Limnol. Oceanogr. 51, 2084–2091. https://doi.org/10.4319/lo.2006.51.5.2084.
Schumann, E.H., 1999. Wind-driven mixed layer and coastal upwelling processes off the south coast of South Africa. J. Mar. Res. 57, 671–691. https://doi.org/10.1357/002224099321549639.
Silvert, W., Platt, T., 1978. Energy flux in the pelagic ecosystem: a time-dependent equation. Limnol. Oceanogr. 23, 813–816. https://doi.org/10.4319/lo.1978.23.4.0813.
Sourisseau, M., Carlotti, F., 2006. Spatial distribution of zooplankton size spectra on the French continental shelf of the Bay of Biscay during spring 2000 and 2001. J. Geophys. Res. 111 https://doi.org/10.1029/2005JC003063.
Sprules, W.G., Barth, L.E., 2015. Surfing the biomass size spectrum: some remarks on history, theory, and application. Can. J. Fish. Aquat. Sci. 73, 477–495. https://doi.org/10.1139/cjfas-2015-0115.
Sun, S., Huo, Y., Yang, B., 2010. Zooplankton functional groups on the continental shelf of the yellow sea. Deep Sea Res. Part II Top. Stud. Oceanogr. 57, 1006–1016. https://doi.org/10.1016/j.dsr2.2010.02.002.
Swart, V.P., Largier, J.L., 1987. Thermal structure of Agulhas Bank water. S. Afr. J. Mar. Sci. 5, 243–252. https://doi.org/10.2989/025776187784522153.
Takahashi, K., Ichikawa, T., Fukugama, C., Yamane, M., Kakehi, S., Okazaki, Y., Kubota, H., Furuya, K., 2015. In situ observations of a doliolid bloom in a warm water filament using a video plankton recorder: bloom development, fate, and effect on biogeochemical cycles and planktonic food webs. Limnol. Oceanogr. 60, 1763–1780. https://doi.org/10.1002/lno.10133.
Thor, P., Dam, H.G., Rogers, D.R., 2003. Fate of organic carbon released from decomposing copepod fecal pellets in relation to bacterial production and ectoenzymatic activity. Aquat. Microb. Ecol. 33, 279–288. https://doi.org/10.3354/ame033279.
Valdes, J.L., Roman, M.R., Alvarez-Ossorio, M.T., Gauzens, A.L., Miranda, A., 1990. Zooplankton composition and distribution off the coast of Galicia, Spain. J. Plankton Res. 12, 629–643. https://doi.org/10.1093/plankt/12.3.629.
Vandromme, P., Nogueira, E., Huret, M., Lopez-Urrutia, A., González-Nuevo González, G., Sourisseau, M., Petitgas, P., 2014. Springtime zooplankton size

structure over the continental shelf of the Bay of Biscay. Ocean Sci. 10, 821–835. https://doi.org/10.5194/os-10-821-2014.

Vandromme, P., Stemmann, L., Garcìa-Comas, C., Berline, L., Sun, X., Gorsky, G., 2012. Assessing biases in computing size spectra of automatically classified zooplankton from imaging systems: a case study with the ZooScan integrated system. Methods Oceanogr. 1–2, 3–21. https://doi.org/10.1016/j.mio.2012.06.001.

Verheye, H.M., Hutchings, L., Huggett, J.A., Carter, R.A., Peterson, W.T., Painting, S.J., 1994. Community structure, distribution and trophic ecology of zooplankton on the Agulhas Bank with special reference to copepods. South Afr. J. Sci. 90, 154–165.

Visser, A., Fiksen, Ø., 2013. Optimal foraging in marine ecosystem models: selectivity, profitability and switching. Mar. Ecol. Prog. Ser. 473, 91–101. https://doi.org/10.3354/meps10079.

Walters, T.L., Lamboley, L.M., López-Figueroa, N.B., Rodríguez-Santiago, Á.E., Gibson, D.M., Frischer, M.E., 2019. Diet and trophic interactions of a circumglobally significant gelatinous marine zooplankter, Dolioletta gegenbauri (Uljanin, 1884). Mol. Ecol. 28, 176–189. https://doi.org/10.1111/mec.14926.

Weidberg, N., Porri, F., Von der Meden, C.E.O., Jackson, J.M., Goschen, W., McQuaid, C. D., 2015. Mechanisms of nearshore retention and offshore export of mussel larvae over the Agulhas Bank. J. Mar. Syst. 144, 70–80. https://doi.org/10.1016/j.jmarsys.2014.11.012.

Welschmeyer, N.A., 1994. Fluorometric analysis of chlorophyll a in the presence of chlorophyll b and pheopigments. Limnol. Oceanogr. 39, 1985. https://doi.org/10.4319/lo.1994.39.8.1985, 1992.

Yebra, L., Berdalet, E., Almeda, R., Pérez, V., Calbet, A., Saiz, E., 2011. Protein and nucleic acid metabolism as proxies for growth and fitness of *Oithona davisae* (Copepoda, Cyclopoida) early developmental stages. J. Exp. Mar. Biol. Ecol. 406, 87–94. https://doi.org/10.1016/j.jembe.2011.06.019.

Yebra, L., Harris, R.P., Smith, T., 2005. Comparison of five methods for estimating growth of *Calanus helgolandicus* later developmental stages (CV–CVI). Mar. Biol. 147, 1367–1375. https://doi.org/10.1007/s00227-005-0039-9.

Yebra, L., Hernández-León, S., 2004. Aminoacyl-tRNA synthetases activity as a growth index in zooplankton. J. Plankton Res. 26, 351–356. https://doi.org/10.1093/plankt/fbh028.

Yebra, L., Kobari, T., Sastri, A.R., Gusmão, F., Hernández-León, S., 2017a. Advances in biochemical indices of zooplankton production. In: Curry, B.E. (Ed.), Advances in Marine Biology. Academic Press, pp. 157–240. https://doi.org/10.1016/bs.amb.2016.09.001.

Yebra, L., Putzeys, S., Cortés, D., Mercado, J.M., Gómez-Jakobsen, F., León, P., Salles, S., Herrera, I., 2017b. Trophic conditions govern summer zooplankton production variability along the SE Spanish coast (SW Mediterranean). Estuar. Coast Shelf Sci. 187, 134–145. https://doi.org/10.1016/j.ecss.2016.12.024.

Zhou, M., 2006. What determines the slope of a plankton biomass spectrum? J. Plankton Res. 28, 437–448. https://doi.org/10.1093/plankt/fbi119.

Zhou, M., Huntley, M.E., 1997. Population dynamics theory of plankton based on biomass spectra. Mar. Ecol. Prog. Ser. 159, 61–73. https://doi.org/10.3354/meps159061.

Zhou, M., Tande, K.S., Zhu, Y., Basedow, S., 2009. Productivity, trophic levels and size spectra of zooplankton in northern Norwegian shelf regions. Deep Sea Res. Part II Top. Stud. Oceanogr. 56, 1934–1944. https://doi.org/10.1016/j.dsr2.2008.11.018.

Zhou, M., Zhu, Y., Peterson, J.O., 2004. In situ growth and mortality of mesozooplankton during the austral fall and winter in Marguerite Bay and its vicinity. Deep Sea Res. Part II Top. Stud. Oceanogr. 51, 2099–2118. https://doi.org/10.1016/j.dsr2.2004.07.008.

Zhu, Y., Tande, K.S., Zhou, M., 2009. Mesoscale physical processes and zooplankton transport-retention in the northern Norwegian shelf region. Deep Sea Res. Part II Top. Stud. Oceanogr. 56, 1922–1933. https://doi.org/10.1016/j.dsr2.2008.11.019.